#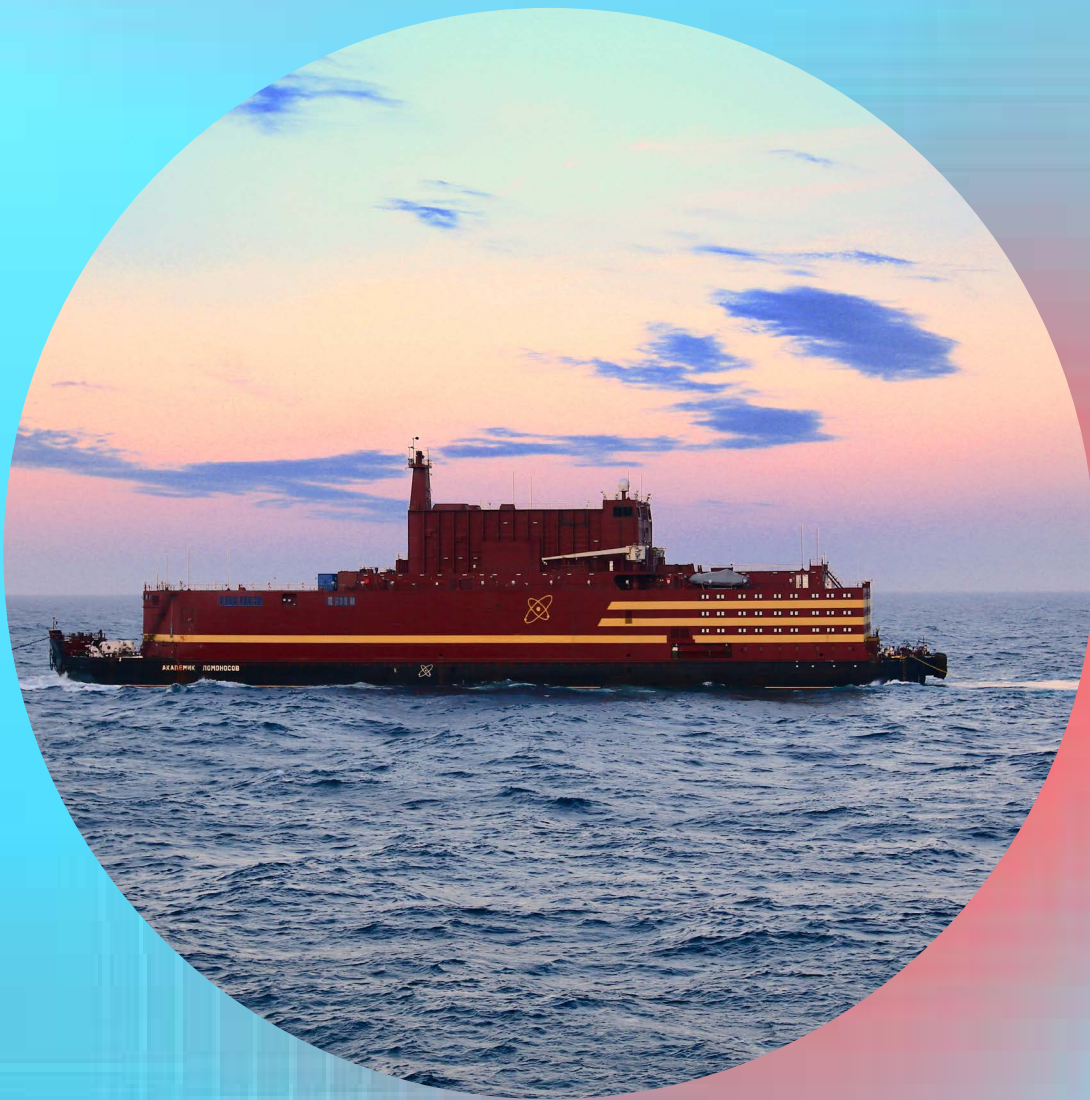 Potential Dispersal of Contaminants from Hypothetical Accidents Involving the Floating Nuclear Power Plant: Akademik Lomonosov

⫙⫙DSA

Norwegian Radiation and
Nuclear Safety Authority

Emneord

Flytende kraftverk, miljømodellering, radioaktiv kontaminasjon.

Resymé

Potensialet for forurensning ble studert for flere hypotetiske scenarier der radioaktivitet ble sluppet ut fra det flytende atomkraftverket Akademik Lomonosov.

Key words

Floating nuclear power plant, environmental modelling, radioactive contamination

Abstract

The potential for contamination was studied for several hypothetical scenarios where radioactivity was released from the floating nuclear power plant Akademik Lomonosov.

Prosjektleder: Ingar Amundsen.

Godkjent:

Sara Skodbo, avdelingsdirektør, avdeling internasjonal atomsikkerhet og kunnskapsutvikling

Potential Dispersal of Contaminants from Hypothetical Accidents Involving the Floating Nuclear Power Plant: Akademik Lomonosov

Table of Content

1   Introduction

1.1   Akademik Lomonosov

Akademik Lomonosov (Russian: Академик Ломоносов) is a barge that was built and operates as the first Russian floating nuclear power plant (FNPP) at the Arctic town of Pevek in Chukotka Autonomous Okrug, Russia, Akademik Lomonosov provides heat to the town and supplies electricity to the regional power grid. The keel of the FNPP was laid in April of 2007 at the Sevmash Plant in Severodvinsk, construction being transferred to the Baltiysky Zavod shipyard in Saint Petersburg in August of 2008. The reactors, KLT-40S units designed by OKBM Afrikander, were delivered in 2009 and they were installed in October 2013. On 28 April 2018, the FNPP left St. Petersburg and was towed to Murmansk for loading of nuclear fuel where it arrived on 17 May 2018. The 5000 km journey to its ultimate destination was begun on 23 August 2019 and it arrived on 9 September 2019. The FNPP commenced operation on 19 December 2019, having been fully commissioned by May of 2020. Supply of thermal power to Pevek had commenced by June of that year.

The barge is 144 meters long and 30 meters wide with a displacement of 21,500 tonnes. The power plant consists of two KLT-40S reactors which are based upon reactor designs for icebreakers. Together these reactors provide 300 MW of thermal power and 70 MW of electrical power. The KLT-40S utilize a low-enriched uranium (LEU) fuel of 14.1% average enrichment and the fuel cycle is 3 years. Spent nuclear fuel is intended to remain on board the FNPP being stored first in a storage pool and then in dry storage casks. Every twelve years the FNPP is to be towed to a special facility for maintenance at which point the spent nuclear fuel built up over the 12-year period is to be removed.

This report analyses the potential for marine or atmospheric dispersion of contaminants released during an accident involving the FNPP. Analysis is conducted for releases at the current location of the FNPP and at a selection of points along a likely route for the FNPP during its return for maintenance. For this purpose, it is assumed that Murmansk will be the likely site of maintenance operations to be conducted on the FNPP.

2   Marine Dispersion

To support the assessment of potential consequences regarding the dispersion of radioactively contaminated water masses into regions of Norwegian interest, an investigation of relevant oceanographic circulation and advection pathways was performed. Naturally, ocean circulation cannot be forecasted accurately for the coming decades, as it depends to a large extent on the development of the atmospheric circulation patterns on the large pan-Arctic scale (e.g., Proshutinsky et al, 2009) and due to the fact that natural variability of the atmospheric circulation, and thus in the ocean, is large. Even attempts to make decadal forecasts based on observed initial states show limited or no accuracy in the Arctic (e.g., Guemas et al., 2016 and references therein). On the other hand, the situation in the forthcoming period 2020 – 2031 is not expected to differ significantly from the present-day situation. A somewhat lower sea ice extend in summer may be expected, if the current long-term trend continues, but also here the natural level of variability is high (Serreze and Stroeve, 2015).

Therefore, it was decided to make use of hindcast simulations of the past decades to investigate principal ocean circulation patterns and to pick two 12-year periods which cover the range of dispersion patterns that transport dissolved pollutants within ocean currents from the region of Pevek to Norwegian waters. Validation of model circulation in the interior Arctic basins is hampered by the lack of observational data. However, the hindcast simulations performed with NAOSIM, the model used for this study, have been validated with available ^{129}I tracer data. This radionuclide, released from the nuclear fuel reprocessing facilities in La Hague and Sellafield, is an excellent tracer to detect and document changes in the large-scale circulation patterns in the Arctic basin (Smith at al., 1999, 2011; Karcher et al., 2012).

In addition, a long-term tracer experiment with a Pacific Water tracer (1948-2018) was performed. Pacific Water enters the Arctic Ocean via the Bering Strait, passing by the East Siberian shelf in close proximity to Pevek. A comparison of the Pacific Water tracer results with available estimates of Pacific Water abundances in the central basin and Fram Strait allows some validation of the model experiment and allows a degree of confidence in the release experiments from Pevek. At the same time the Pacific Water tracer experiment enables investigation of the large-scale circulation patterns in the central Arctic, as they are relevant for a potential release from Pevek and support the selection of the two 12-year periods which were used for the release experiments. Figures 1 to 3 present release locations used in this study, the Northern Sea Route and Northern Sea Route shipping traffic for all vessels for the period Jan – Dec 2016, respectively. Red dots in Figure 1 mark the location of the release locations use in this study. From East to West: Off Pevek, North of East Siberian Islands, North of Severnaya Zemlya, and North of Novaya Zemlya. Blue dots mark the locations of the time series shown in the text: North, East and South of Svalbard, in the central Barents Sea and at the North Cape.
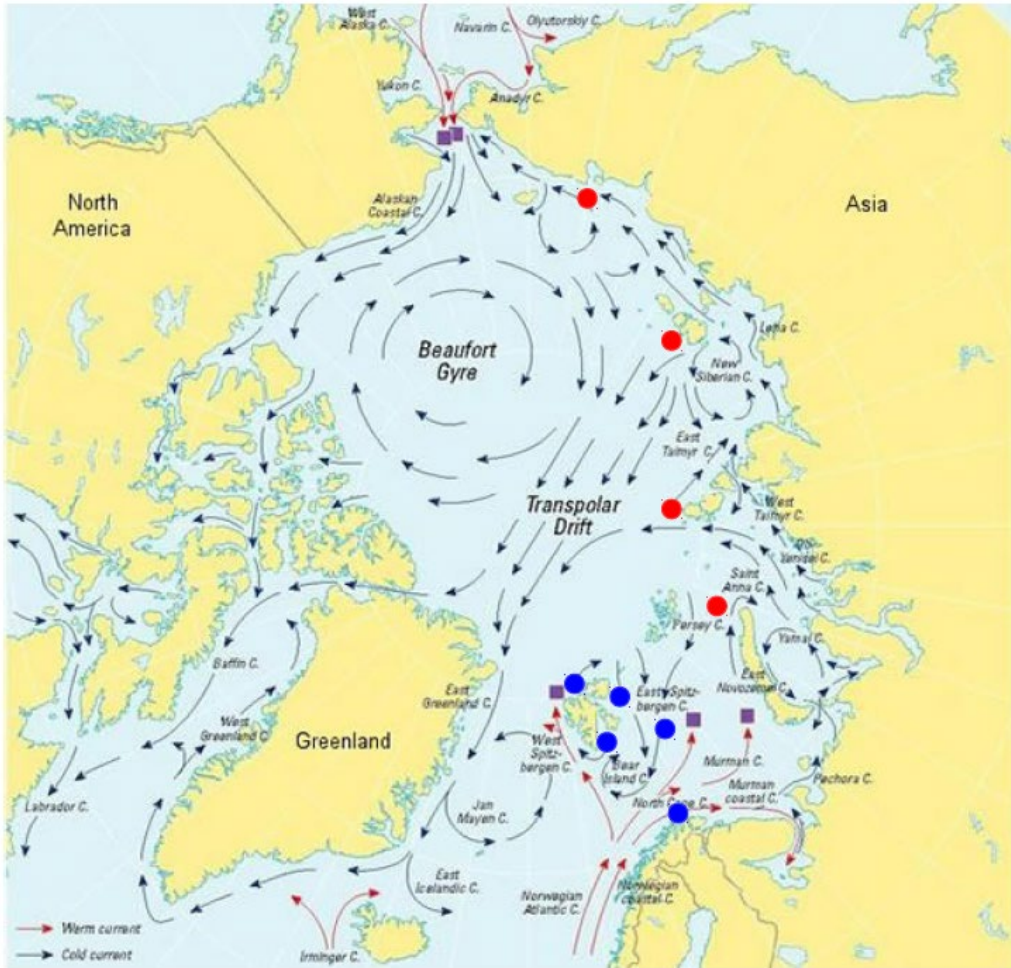
Figure 1: Map of the Arctic Ocean showing the mean surface circulation, AMAP (1998).

Figure 2: The Northern Sea Route, showing selected NSR route alternatives (Brubaker and Ragner, 2010).
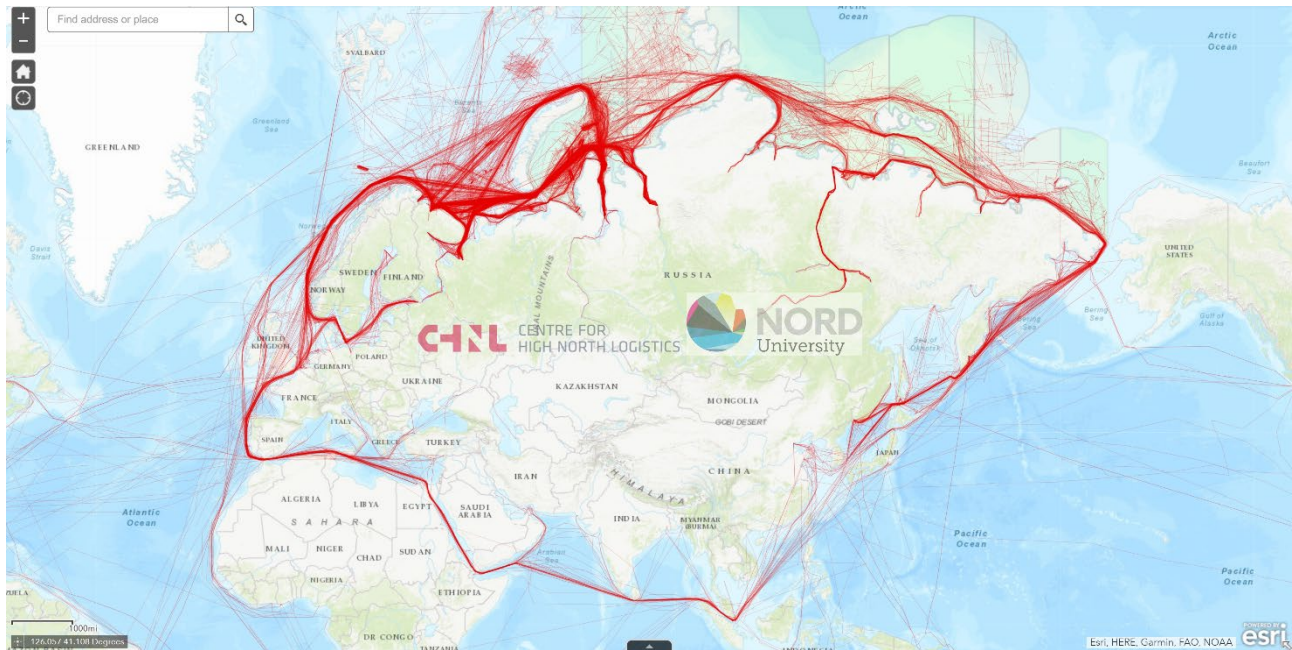
Figure 3: Map of the Northern Sea Route showing shipping traffic, all vessels for the period Jan – Dec 2016 (CHNL Information Office of the Center for High North Logistics and Nord University, http://arctic-lio.com/?p=1240, 2018)

2.1 Model description

The model experiments are performed with NAOSIM (North Atlantic-Arctic Ocean-Sea Ice Model), a regional, coupled sea ice-ocean model, developed at the Alfred Wegener Institute for Polar and Marine Research (Köberle and Gerdes, 2003). It is derived from the Geophysical Fluid Dynamics Laboratory modular ocean model MOM-2 (Pacanowski, 1995) and a dynamic-thermodynamic sea ice model with a viscous-plastic rheology (Hibler, 1979). NAOSIM has been used for numerous studies on the dynamics of the Arctic Ocean and the Nordic Seas (e.g., Gerdes et al., 2001; Kauker et al., 2003; Karcher et al., 2003). It has also been previously applied to studies of the dispersion of tracers (Gerdes et al., 2001; Karcher et al., 2004, 2012, 2017). In this study a version with 30 vertical, unevenly spaced layers are used. The surface layers have a thickness of 20 m. The model domain encompasses the Arctic Ocean, the Nordic Seas and the Northern Atlantic Ocean north of approximately 50°N. At the open Bering Strait a net input volume inflow from the Pacific Ocean is introduced of 0.8 Sverdrups. At the Southern boundary and in the Bering Strait, open boundary conditions have been implemented following Stevens (1991), thereby allowing the outflow of tracers and the radiation of waves. The initial hydrography in January 1948 is adopted from the PHC winter climatology (Steele et al., 2001), while a yearly mean climatology is used as a reference for surface salinity restoring on a time scale of 180 days. The restoring of sea surface salinity is a common method used to prevent the ocean salinity from drastically drifting away from the observed ocean state (Steele et al., 2001). Sea surface salinity restoring compensates for a mismatch between freshwater forcing data (e.g., precipitation and runoff) and model physics. In the absence of restoring the model drift is arbitrary, depending on the combination of forcing data set and model physics. The model is driven with daily atmospheric forcing from 1948 to 2017 (NCEP/NCAR reanalysis (Kalnay et al., 1996)).

The tracer release to track water of Pacific origin is implemented by setting the concentration of Pacific Water to unity along a section crossing the strait. Due to the formulation of NAOSIM as a rigid-lid model, volume is conserved. This means that parameterization of river runoff is employed using negative salt fluxes proportional to seasonal climatology of runoff for each of the major rivers which follows the AOMIP

protocol (Holloway et al., 2007). Also, the sea ice melt and precipitation are employed using negative salt fluxes. As a consequence, the pacific water tracer concentration in the model experiment is not diluted by runoff, sea ice melt or precipitation.

The experiment with the artificial Pacific Water tracer does not serve as a means to validate the Arctic large-scale circulation in the simulation. It allows tracking the dispersion of water which has been entering through the Bering Strait and moved over on the East Siberian Shelf, passing nearby Pevek, through the Arctic Ocean. It thus can serve as an indicator of the potential dispersion pathway for the release of dissolved, conservative substances through the Arctic Ocean. For a number of years, estimates for the location of the boundary of Pacific Water with the Atlantic Water dominated domain are available. Even more extensive is a time series of derived Pacific water fraction in Fram Strait, which covers the period 1990 – 2017 (Dodd et al., in prep).

2.2 Oceanographic context

The large-scale circulation at the surface of the Arctic Ocean is dominated by two features: the Beaufort Gyre, a clockwise gyre that occupies large parts of the Amerasian Basin between the Lomonosov Ridge and the North American continent, and the Transpolar Drift Stream that carries water from the East Siberian and Laptev Sea shelves to Fram Strait (Proshutinsky et al., 2009) (Fig. 1). From the Pacific Ocean this system is fed by waters entering through the Bering Strait. These move on to the Chukchi and East Siberian shelves, and partly move into the Transpolar Drift and the Beaufort Gyre. They subsequently leave the Arctic via the East Greenland Current through the Fram Strait. Another fraction of the Pacific Water moves to the East and exits through the Canadian Arctic Archipelago (Jones et al., 1986). Water of Atlantic origin enters on the Eastern side of Fram Strait and via the Barents Sea. The latter mixes with Siberian River water that feeds on to the shelves of the Kara Sea and the Laptev Sea, moving towards the Northeast and entering the Eurasian Basin, that is located between the Lomonosov Ridge and the western Siberian shelves. These waters finally feed into the Transpolar Drift on the Siberian flank to also exit through Fram Strait.

All releases of soluble substances such as radionuclides in the Arctic Ocean would be carried by this current system, and its pathway would be determined by the location of release. However, the current system as described is not constant in time. The intensity of the Beaufort Gyre circulation for example is subject to wind-driven fluctuations on a seasonal to pentanal timescale, as described by Proshutinsky et al. (2009). A drastic restructuring of the Arctic Ocean hydrography and circulation as a consequence of the high state of the atmospheric circulation pattern called 'Arctic Oscillation (AO)' 1988-1995 has been described elsewhere (McLaughlin et al., 1996; Carmack et al., 1997; Steele at al., 2004). At the surface it led to a shrinking of the Beaufort Gyre to a size barely covering the Beaufort Sea. The axes of the Transpolar Drift shifted from an orientation parallel to the Lomonosov Ridge, stretching from the East Siberian and Laptev Sea slope to Fram Strait, to one stretching from the Chukchi Plateau to Fram Strait. One of the consequences of this restructuring was a strong release of fresh surface water from the Beaufort Gyre into the North Atlantic (Karcher et al., 2005). At the surface, as well as in the deeper layers, this was accompanied by an intrusion of Atlantic derived water from the West far into the Makarov Basin and even the Canada Basin. This was shown by hydrography data and observed anthropogenic tracer distribution from the AOS 1994 section and the SCICEX cruises (Carmack et al., 1997; Smith et al., 1998, 1999). Model simulations with the same model used here supported the picture suggested by these observations and put them into a larger scale context of changing circulation patterns (Karcher et al., 2012).

The restructuring also had consequences for the distribution and the pathways of Pacific Water in the Arctic. It meant an Eastward shift of the front with the Atlantic derived water, which was found to be located over the Western slope of the Chukchi plateau during the SCICEX' 93 expedition (McLaughlin et al., 1994; Steele et al., 2004). Data from the AOS94 section, occupied one year later, indicated that a large part of the Pacific Water moved Westward to the Chukchi plateau and beyond. Ekwurzel et al. (2001) reported high concentrations of Pacific Water reaching more than 40% off the Chukchi slope at the surface and a maximum of > 50% at 75-100m depth. Further into the basin they found the front between the Pacific derived water and Atlantic origin water just South of the Lomonosov Ridge in the Canada Basin near the North Pole. Very little was known about the distribution of Pacific Water in the interior Arctic basins until 2005. From hydrographic measurements it is known that the Transpolar Drift and the Beaufort Gyre started returning to the old extension and location, respectively, in the early 2000s (Björk et al, 2002). It is concluded that this also shifted the border between Pacific and Atlantic derived water back to the old location.

2.2.1 Supporting Pacific Water tracer experiment

The dispersion of Pacific Water was simulated from 1948 to 2018. A basic feature of the distribution of the Pacific Water until the late 1980s is a low Pacific Water concentration in the center of the Beaufort Gyre (Fig's 4 and 2). High concentrations were observed in the Transpolar Drift, and due to cyclonic recirculation into the Canadian Basin before it reached Fram Strait. Concentrations are also high North of the Canadian Archipelago and the Greenland coast. This indicates a rather long ventilation time for the interior Beaufort Gyre in our simulation, which is consistent with experiments of Stewart and Haine (2013). Their experiments indicate an adjustment time for the Beaufort Gyre freshwater content to a constant wind forcing of 10-20 years. Large scale meandering of the Transpolar Drift, as it is outlined by high Pacific Water fractions, is apparent as well as relocation or bending of the Transpolar Drift's main axis (Fig 4). For the 1960s to the late 1980s the general orientation for the Transpolar Drift, and thus the front between waters derived from the Pacific and the Atlantic, respectively, is located near the Lomonosov Ridge. This is consistent to the location of the front in the early 1980s as it was deduced from measurements of nutrients which mark Pacific waters (Jones and Anderson 1986).

Observations in 1993 (McLaughlin et al., 1994) indicated the position of the Transpolar drift, as marked by a strong front between the hydrographic characteristics of the waters of Pacific versus Atlantic origin, was located in the Western parts of the Makarov Basin, not far from the slope of the Mendeleev Ridge. Confirming this result with a more extensive observational program as part of the AOS 94 expedition in 1994 from the Bering Strait via the North Pole to the Western Eurasian basin, the front of Pacific Water with the Atlantic derived water masses which delineates the location of the Transpolar Drift was located over the Western slope of the Mendeleev Ridge near 180ºE (Ekwurzel et al., 2001). Figure 4k, 1994, shows that the model covers the far Western location of the front very well. Furthermore, in the mid-1990s observations of the radionuclide [129]I, which in the Arctic Ocean can be used as a marker for water of Atlantic origin also showed the location of the Pacific Water/Atlantic Water front at the surface in the same region (Smith et al., 1999). Results from the same model setup used here for the simulation of [129]I showed a very good comparison with the observation (Karcher et al., 2012). A decade later, in 2005, a section crossing the basin from Alaska to the North Pole, found Pacific Water extending beyond the Alpha Ridge almost reaching the North Pole (Jones et al., 1986), with highest surface values over the Alpha Ridge. Two to three years later, [129]I observations from 2007 to 2009, though fewer than in the 1990s, confirm the location of the Pacific derived water/Atlantic derived water from between the Alpha Ridge and the North Pole. The model experiments for [129]I (Karcher et al, 2012) as well as the Pacific Water tracer

experiments shown here (Fig 5) fit to these results. A large part of the Pacific Water leaves the Arctic with the East Greenland Current moving south through Fram Strait. Observations of Pacific Water abundance in the Strait have been performed in the past on an irregular basis. Dodd et al. (in prep), in continuation of earlier work (Dodd et al., 2012), have gathered all available data required for the calculation of Pacific Water fraction in Fram Strait for the period 1990 to 2017. Most notably, the period between 1999 and 2007 is marked by very low fractions of Pacific Water in the East Greenland Current of Fram Strait in observations as well as in the model experiment.
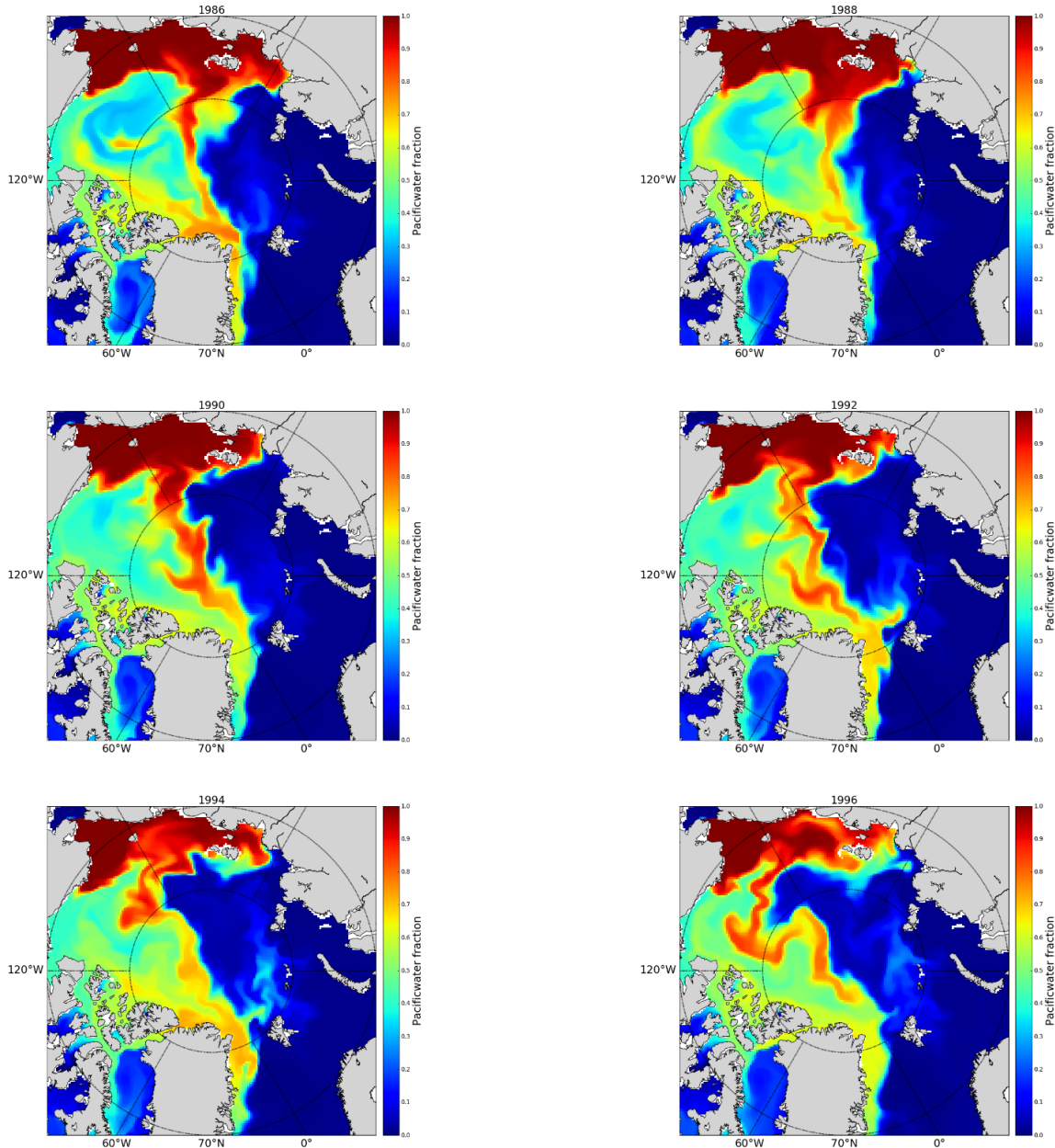

Figure 4: Simulated Pacific Water tracer concentration in the top layer (0-20m) for August 1986, 1988, 1990, 1992, 1994 and 1996.
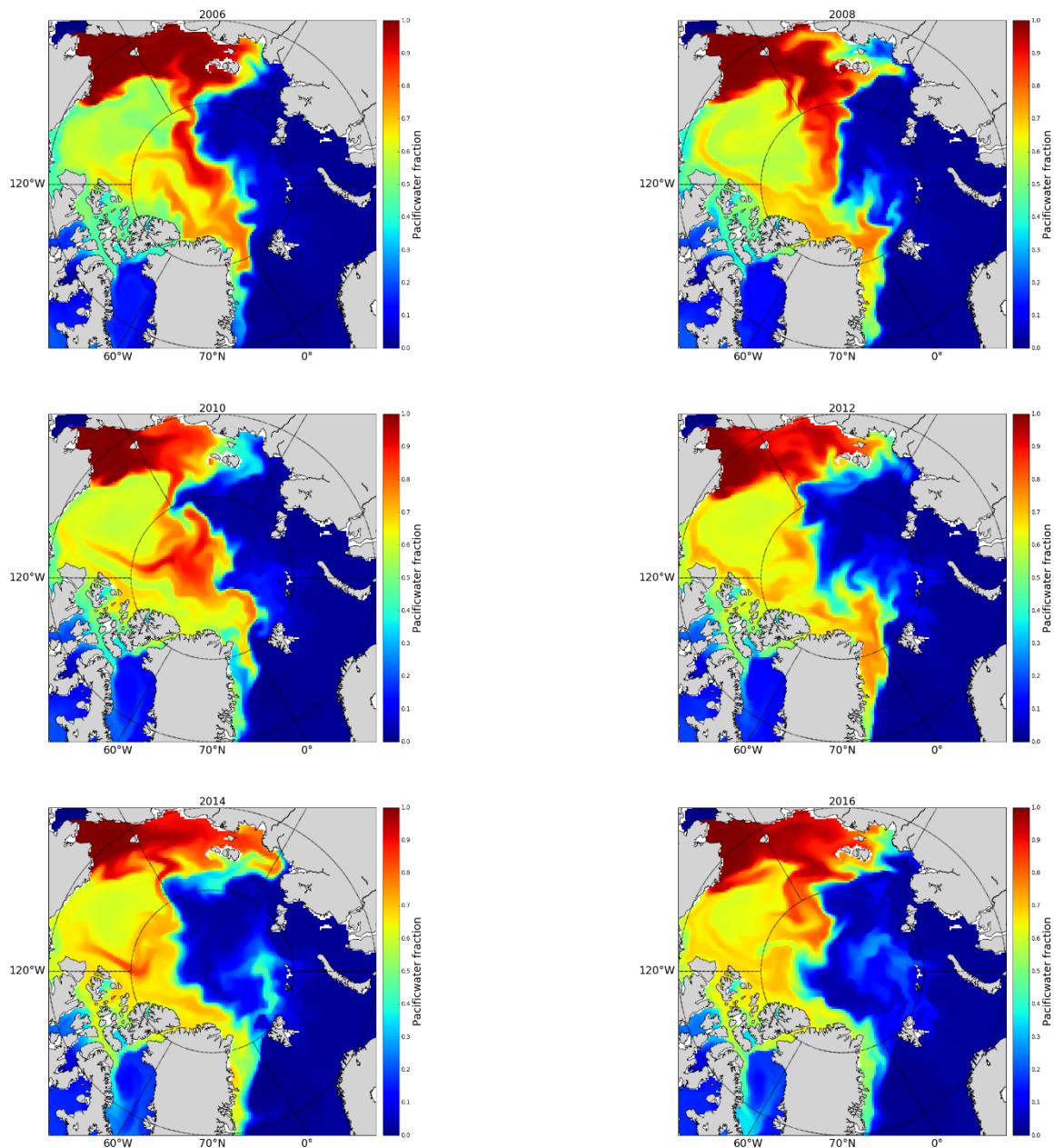
Figure 5: Simulated Pacific Water tracer concentration in the top layer (0-20m) for August 2006, 2008, 2010, 2012, 2014 and 2016.

2.3 Selection of dispersion periods

The results gained with the Pacific Water tracer experiments provide an indication of the fate of water masses transported with the Transpolar Drift from the East Siberian Shelf near Pevek, to Fram Strait, Svalbard and the Western Barents Sea. In particular, it allows identifying periods with intense recirculation events which carry water from the Transpolar Drift Southward towards the North-Western Barents Sea and the Svalbard coast, the regions potentially most affected by the advection of contaminated water from the East Siberian Shelf. Such intense inflow periods of Pacific derived water in the recent decades were found 1994-1996, 2010-2011, 2014-17 for Svalbard and 1994-1998, 2001/2, 2016 for the North-Western Barents Sea.

Therefore, experiment periods for the releases from Pevek as January 1985 to December 1996 and January 2005 to December 2016 were chosen. By doing this, the periods would cover the intense inflow periods/events with sufficient head time for the contaminated water masses to the Norwegian waters.

2.4 Release scenarios

Experiment periods for the simulation of hypothetical releases were chosen as January 1985 to December 1996 and January 2005 to December 2016. To capture the uncertainty due to releases starting in summer, three experiments from June 2005 to June 2017 were also performed.

Releases for the location off Pevek (1), the location of the power plant's planned operation, were calculated as well as three locations en route from/to Murmansk. The actual route of the transfer is unknown, so the study therefore relies on published routes for the Northern Sea Route passages. Figure 2 shows such alternative routes for the Northern Sea Route. In the interest of investigating possible 'worst case' releases, three positions along possible routes of the NSR were chosen that have a high potential to carry contaminated water towards Norwegian waters. The circulation of water masses on the East Siberian shelves typically is directed Eastward and thus away from Norway. In contrast in the deep interior Arctic Basin, off the shelf break, the circulation is dominated by the Transpolar Drift and typically directed towards Fram Strait (see section 2), and thus towards waters of Norwegian interest. Release locations were therefore chosen as follows: (2) North of the New Siberian Islands, a route that is often taken already in present day conditions (Fig. 3, NSR all ship motions in 2016); (3) North of Severnaya Zemlya, placed on a route far North that is rather unlikely under current conditions, but may be an option if a transport would encounter weak sea ice conditions and would try to avoid the near coast passages; (4) A route closer to Norwegian waters, namely North of Novaya Zemlya, quite obviously one of the main routes for the NSR passages nowadays (Fig 3). All experiments encompass continuous releases of 1 TBq/year from all four release locations and instantaneous releases of 1 PBq (10^{15} Bq) from Pevek and North of Severnaya Zemlya (see Table 1 for a complete overview, and Figure 1 for the release locations). For each experiment a surface release and a bottom release have been performed.

Table 1: Overview over the release scenarios, cont = continuous release, inst = instantaneous release, release locations and experimental periods.

Location	Jan 1985 – Dec 1996	Jan 2005 – Dec 2016	June 2005 -July 2017
Pevek	cont, inst	cont, inst	inst
New Siberian Islands	cont	cont	cont
Severnaja Semlja	cont, inst	cont, inst	
Novaya Zemlya	cont	cont	cont

In the following, examples from the surface release scenarios are presented and discussed with respect to the temporal development of the dispersion in the surface layer, as well as time series of surface concentrations in five locations of interest to Norway: North, East and South of Svalbard, in the central Barents Sea, and at the North Cape (Figure 1). The full 3-dimensional results for all experiments are stored as monthly means in NetCDF format on a server and are accessible via a web-based interface.

2.4.1 Jan 1985 – December 1996, continuous releases at the surface

The large-scale circulation in this period is an example for a dramatic size reduction of the Beaufort Gyre and a relocation of the Transpolar Drift. The Drift moves from an orientation parallel to the shelf slopes of the Kara and Barents Sea to a line from the Chukchi slope to the Fram Strait. This forms almost a direct route from the Eastern East Siberian Sea to regions relevant for Norway. This relocation started around 1990 and lasted for 6-8 years, most of which is part of the current simulation period (see section 3). The return to condition similar to before 1990 started in 1998 and is not covered by this set of release experiments.

The release from the location off Pevek, after spreading on the East Siberian Shelf for the first few years, spills over into the deep basin North of Pevek to head towards the North Pole and subsequently into Fram Strait (Fig. 6, upper panels). The surface circulation in the Western Eurasian Basin implies an Eastward recirculation of part of the contaminated water when approaching Fram Strait with the Transpolar Drift. This leads to an arrival of contamination levels around $0.04 \cdot 10^{-2}$ Bq/m^3 North of Svalbard in late 1992, about 8 years after start of the continuous release (Fig. 6, bottom panels). Subsequent recirculation episodes in the autumn/winter seasons of the following years lead to recurring pulses with increased contamination levels of about $0.3 – 0.4 \cdot 10^{-2}$ Bq/m^3 in North of Svalbard. For the regions East of Svalbard a similar level of contamination is reached only once during the simulation period, when a particularly intense recirculation pulse enters the Northern Barents Sea East of Svalbard in winter 1994. Contamination levels South of Svalbard remain lower by about one order of magnitude. Even lower levels occur in the central Barents Sea with a singular peak that reaches concentrations of about $0.001 \cdot 10^{-2}$ Bq/m^3. Concentrations North of the North Cape remain at levels below 10^{-6} Bq/m^3.

The release from the location just North of the New Siberian Islands directly feeds into the Transpolar Drift during the first years of the simulation. With the shift of the Transpolar Drift origin from the Eurasian Basin to the Chukchi Plateau, however, the contaminated water moves Eastward into the Amerasian Basin first, before it travels further towards the North Pole and the Fram Strait (Fig. 7, upper panels). The contaminated water is caught up by the recirculation earlier than in the case of the Pevek release, first peaks with concentrations of above $0.2 \cdot 10^{-2}$ Bq/m^3 arrive North of Svalbard in 1990. The maximum peak occurs in 1993 with $1.2 \cdot 10^{-2}$ Bq/m^3 (Fig. 7, lower panels). Concentrations East of Svalbard and South of Svalbard stay below $1 \cdot 10^{-2}$ Bq/m^3 and $0.2 \cdot 10^{-2}$ Bq/m^3, respectively. For the central Barents Sea and the North Cape concentrations are a magnitude larger than for the release at Pevek.
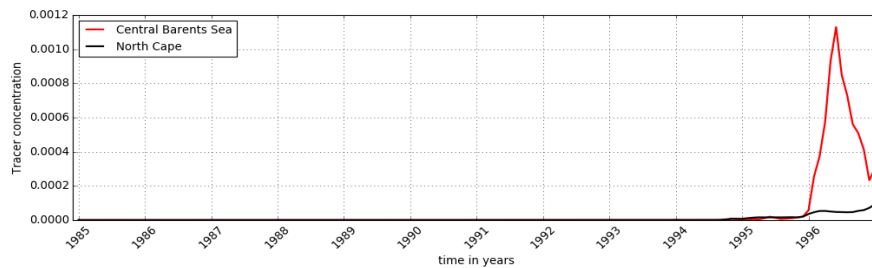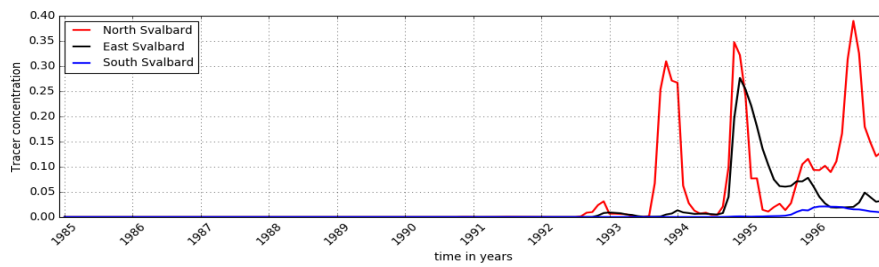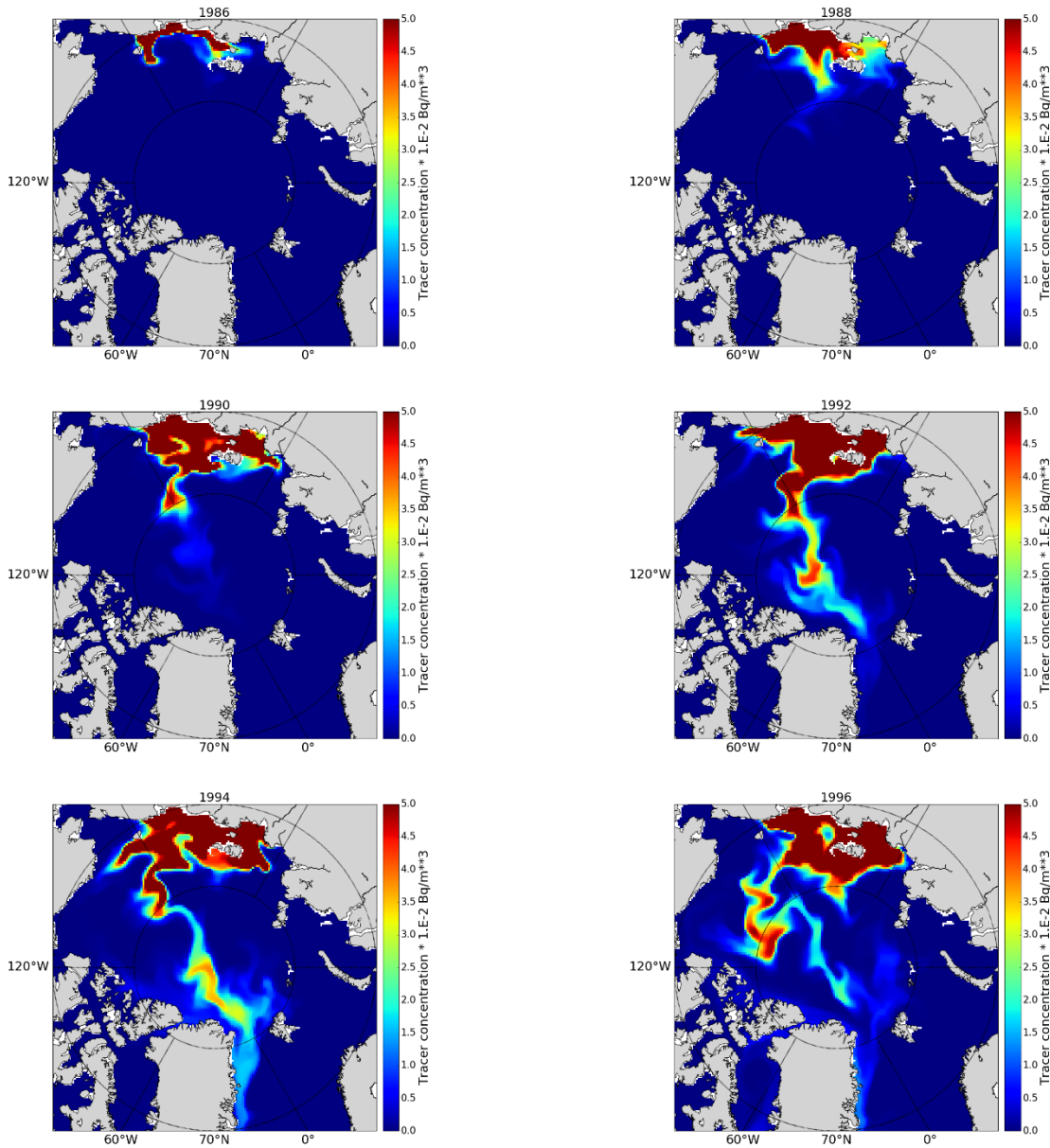
Figure 6: Continuous release of 1 TBq/yr off Pevek (start Jan 1985): concentration in the top 20m. Upper panels: dispersion patterns in December 1986-96; Bottom panels: timeseries at selected locations in Norwegian waters in 10^{-2} Bq/m^3 (see Fig 1).
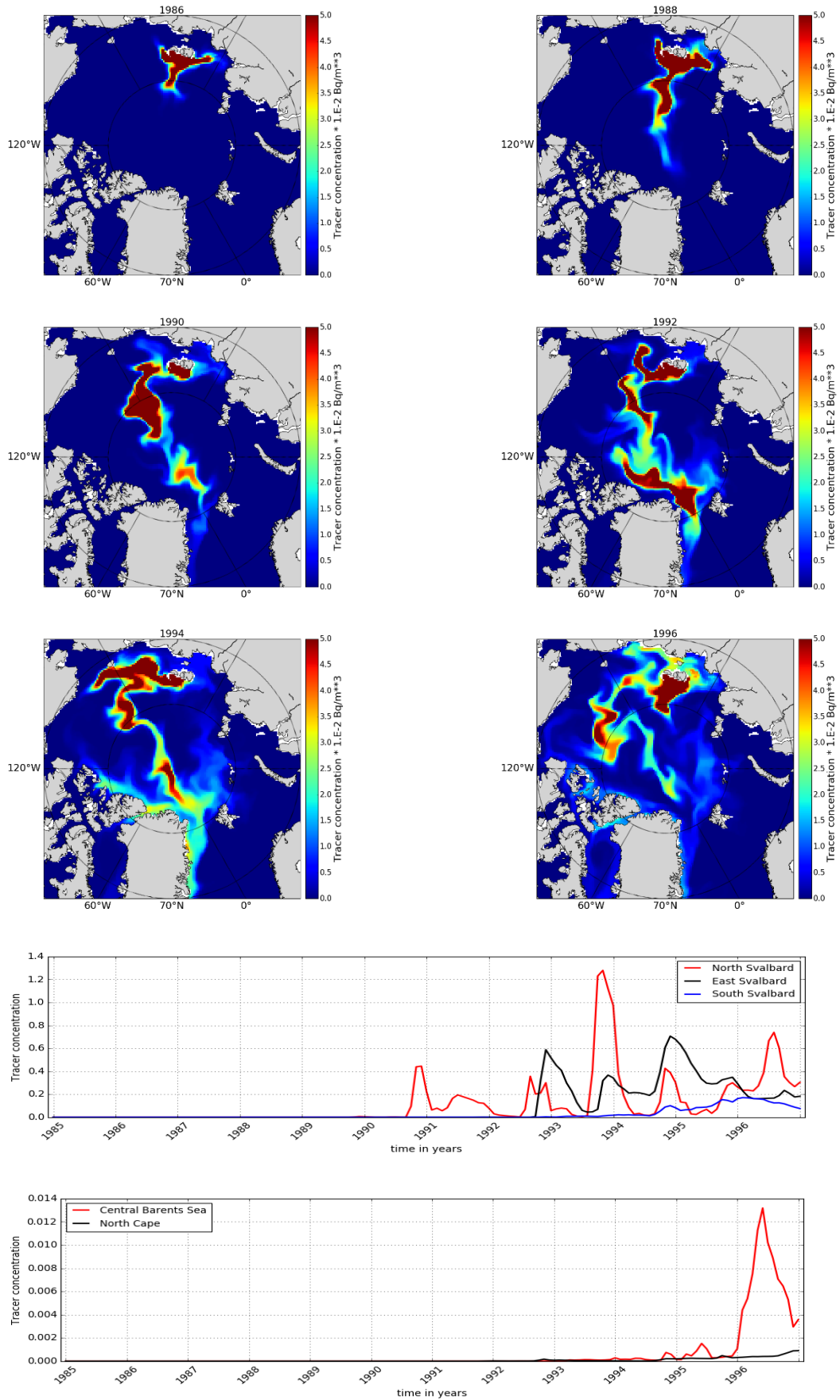
Figure 7: Continuous release of 1 TBq/yr North of the New Siberian Islands (start Jan 1985): concentration in the top 20 m. Upper panels: dispersion patterns in December 1986-96; Bottom panels: timeseries at selected locations in Norwegian waters in 10^{-2} Bq/m^3 (see Fig 1).

Releasing the 1 TBq/yr from the location just North of Severnaya Zemlya ends in similar contamination levels around Svalbard and in the Barents Sea, as for the New Siberian Island release further East. However, a somewhat differing timing takes place, due to the fact that in this case the release occurs into the Atlantic Water domain to the Eurasian side of Transpolar Drift, which leads to a widespread contamination of the Eurasian Basin.

For the release from the location closest to the Norwegian waters North of Novaya Zemlya, the spread of the contamination is distinctly different from the previous cases, as the release occurs on the Siberian shelf at the border between the Barents and the Kara Sea (Fig. 8, upper panels). The plume at the surface dissolves much quicker in comparison to the other cases. The reason is the subduction of the signal to great depths from this location, as a consequence of deep-water formation on the shelf (not shown). While the general direction of the flow at this location is Eastward towards the Northern Kara Sea, reverse flow events to the West take place regularly between the Northern tip of Novaya Zemlya and Franz-Josef-Land for short periods or is caught up by the Westward Persey Current (Fig 1) leading to contaminant levels South and East of Svalbard of up to $0.3 \cdot 10^{-2}$ Bq/m^3 from the late 1980s on (Fig. 8, lower panels). Towards the end of the 12-year simulation, concentrations around Svalbard increase further, as contaminated water which has been taking the loop via the Northern Kara Sea into the Eurasian basin and Southward with the Transpolar Drift, reaches Svalbard with the recirculation North of Fram Strait. This leads to another contaminant peak reaching Svalbard from the North. As for the other release locations a peak in contamination occurs at the central Barents Sea in spring 1996, as a consequence of contaminated Polar Water intruding East of Svalbard from the North.
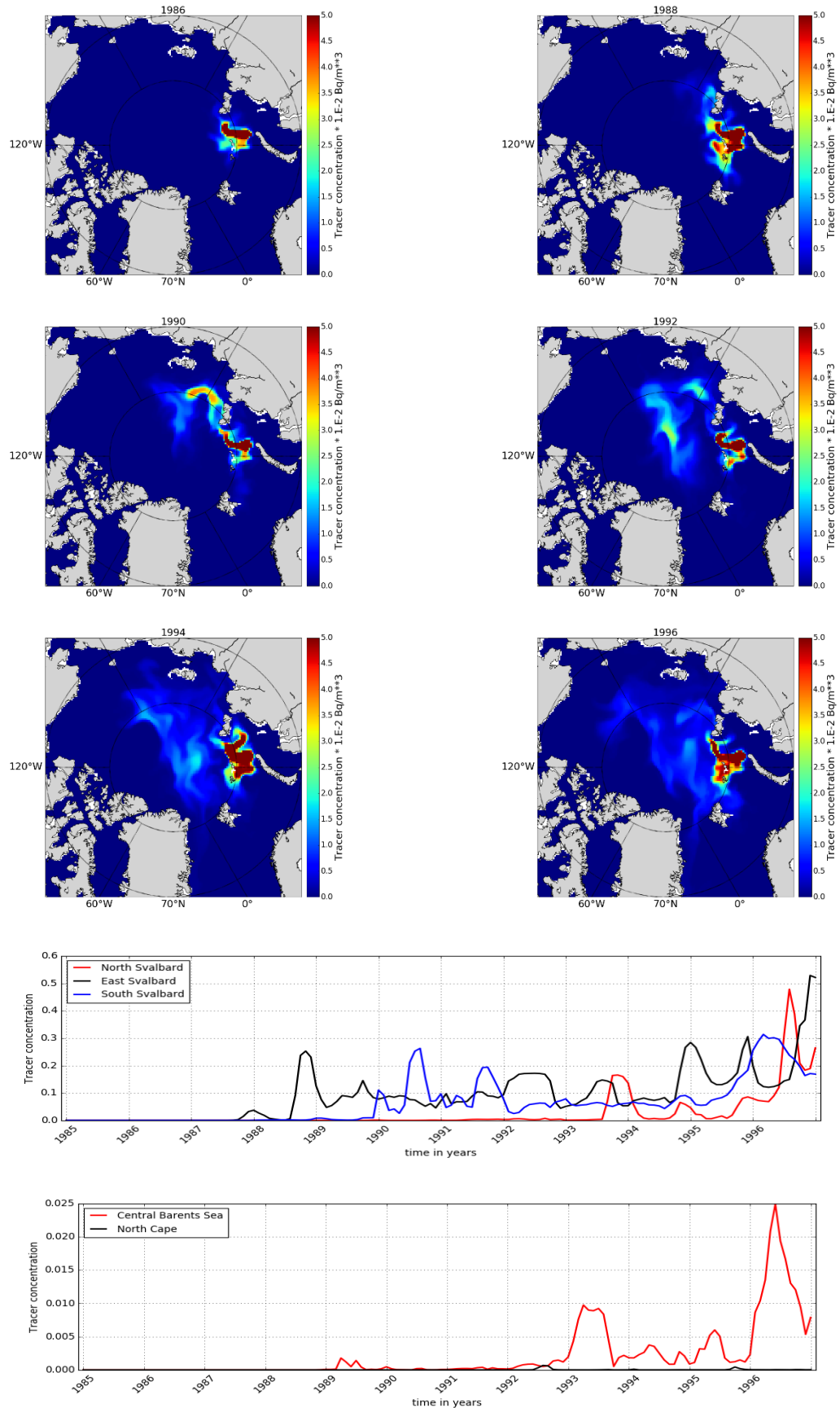
Figure 8: Continuous release of 1 TBq/yr North of Novaya Zemlya (start Jan 1985): concentration in the top 20 m. Upper panels: dispersion patterns in December 1986-96; Bottom panels: timeseries at selected locations in Norwegian waters in 10^{-2} Bq/m^3 (see Fig 1).

2.4.2   Jan 2005 – December 2016, continuous release at the surface

In the first few years the release from the location off Pevek, which started in January 2005, shows a spread on to the East Siberian Shelf (Fig. 9, upper panels), similar to the situation found in the release which started 1985 (compare Fig. 4, upper panels). However, in stark contrast to the 1985-1996 release a period of Eastward dispersion into the Beaufort Sea and onto the Chukchi Shelf occurs for the first few years. Feeding of the Transpolar Drift is weaker than in the period 1985-1996 except for a plume recirculating Westward North of Greenland around 2010. A more intense contamination of the Transpolar drift does not occur before 2015/16. Contamination levels around Svalbard (Fig. 9, bottom panels) show pulses of increased levels against a low background from the 8th year (2012) of dispersion on as in the 1985-1996 experiment with peak values of $0.03 \ 10^{-2}$ Bq/m^3 in 2012/13 to $0.3 \ 10^{-2}$ Bq/m^3 in 2015. For the central Barents Sea and the North Cape maximum concentrations are considerably smaller with up to $3 \ 10^{-6}$ Bq/m^3.

The release from the location just North of the New Siberian Islands also in this release period directly feeds into the Transpolar Drift (Fig. 10, upper panels). In contrast to the 1985-1996 period, however, in this case there is a much more Western path of the Transpolar Drift on the last part of its passage through the Arctic, between the North Pole and Northern Greenland/Fram Strait. This leads to overall lower concentrations around Svalbard. Peak vales on the coast of Svalbard are below $1 \ 10^{-2}$ Bq/m^3 in contrast to $1.4 \ 10^{-2}$ Bq/m^3 in the 1985-1996 case (Fig. 10, bottom panels). For the central Barents Sea and the North Cape barely reach $7 \ 10^{-6}$ Bq/m^3.

Release from the location just North of Severnaya Zemlya shows similar timing and levels of contamination as for the release North of the New Siberian Islands, with slightly higher values though around Svalbard (up to $1.6 \ 10^{-2}$ Bq/m^3), than were found for the same release point in the 1985-1996 period (Fig. 11).

Slightly higher values around Svalbard than in 1985-1996 are also found for the release from the location closest to the Norwegian waters North of Novaya Zemlya. This holds for the East coast of Svalbard, which is impacted by regular and consistent Westward dispersion from the release point North of Novaya Zemlya over longer periods, leading to concentrations of $0.3 \ 10^{-2}$ Bq/m3 and peaks of up to $0.8 \ 10^{-2}$ Bq/m^3 in 2012/13. During this period also enhanced concentrations show up in the central Barents Sea (Fig. 12, bottom panels). For the major fraction of the contaminant Eastward dispersion occurs. As was the case in the period 1985 – 1996 the surface signal quickly dissolves downstream on the way to the Eastern Eurasian Basin as a consequence of deep-water formation in the Eastern Barents Sea and the Northern Kara Sea (Fig. 12, bottom panels).
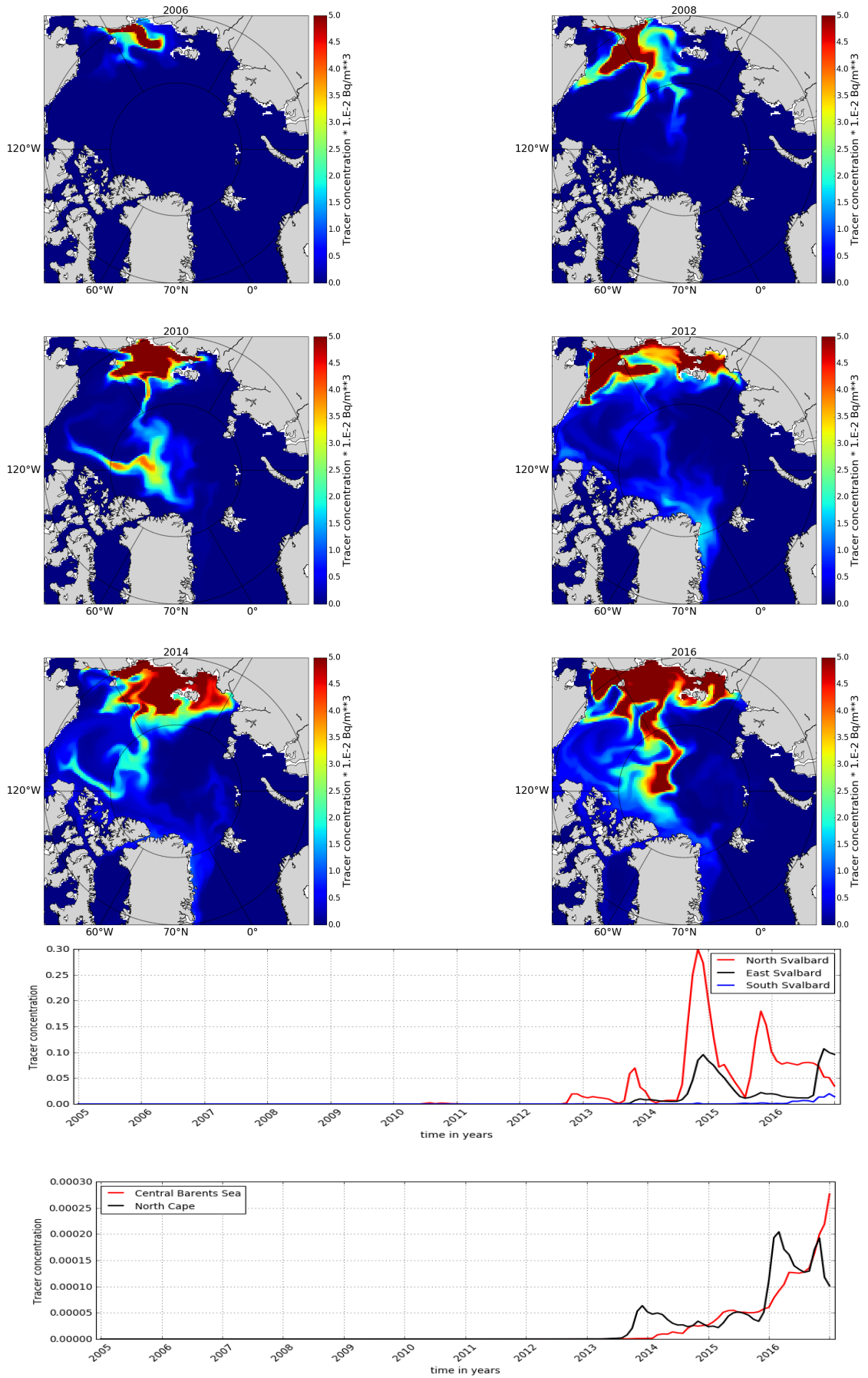
Figure 9: Continuous release of 1 TBq/yr off Pevek (start Jan 2005): concentration in the top 20m. Upper panels: dispersion patterns in December 2006-16; Bottom panels: timeseries at selected locations in Norwegian waters in 10^{-2} Bq/m^3 (see Fig 1).
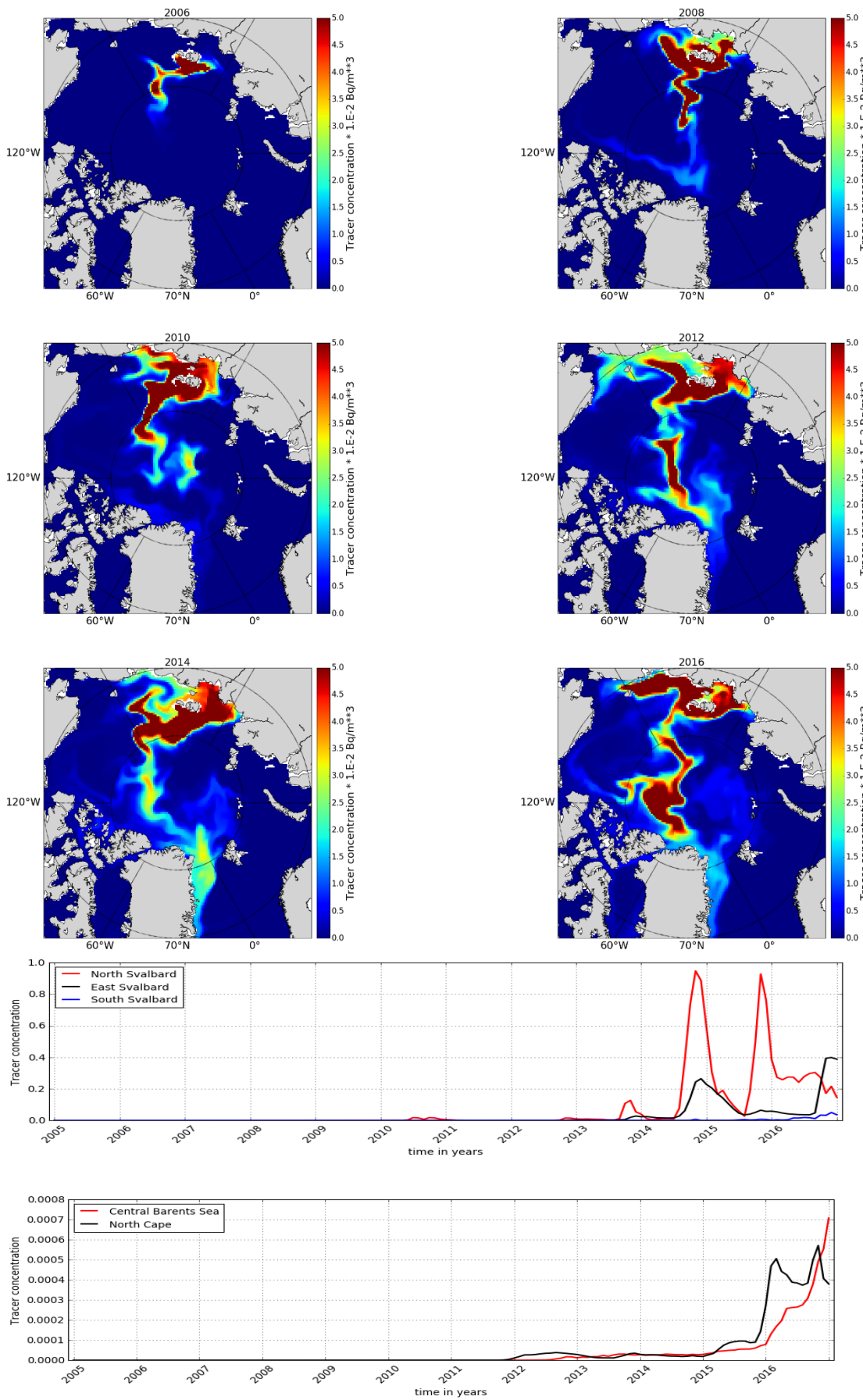
Figure 10: Continuous release of 1 TBq/yr North of the New Siberian Islands (start Jan 2005): concentration in the top 20m. Upper panels: dispersion patterns in December 2006-16; Bottom panels: timeseries at selected locations in Norwegian waters 10^{-2} in Bq/m^3 (see Fig 1).
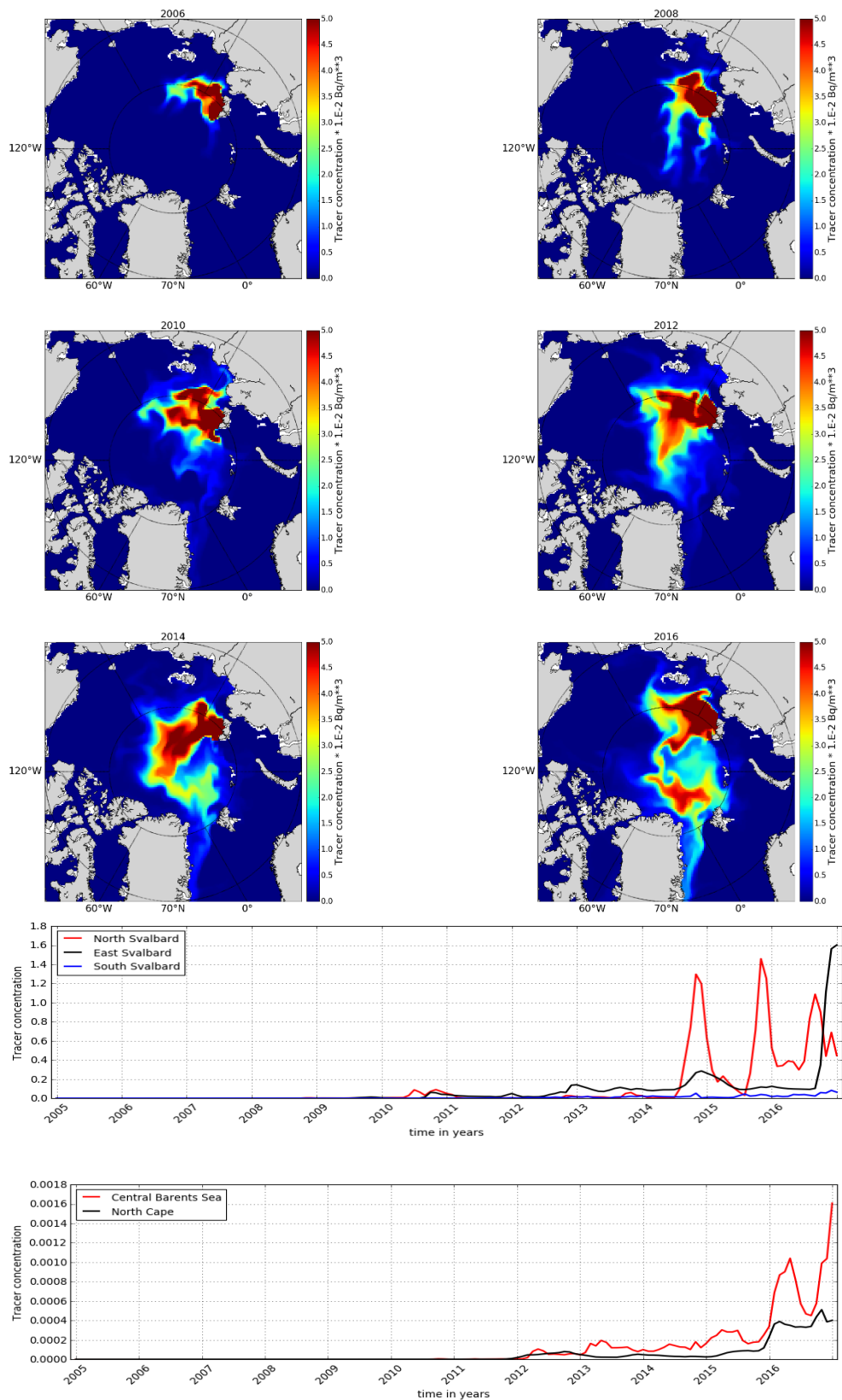
Figure 11: Continuous release of 1 TBq/yr North ofSevernaya Zemlya (start Jan 2005): concentration in the top 20m. Upper panels: dispersion patterns in December 2006-16; Bottom panels: timeseries at selected locations in Norwegian waters in 10^{-2} Bq/m^3 (see Fig 1).
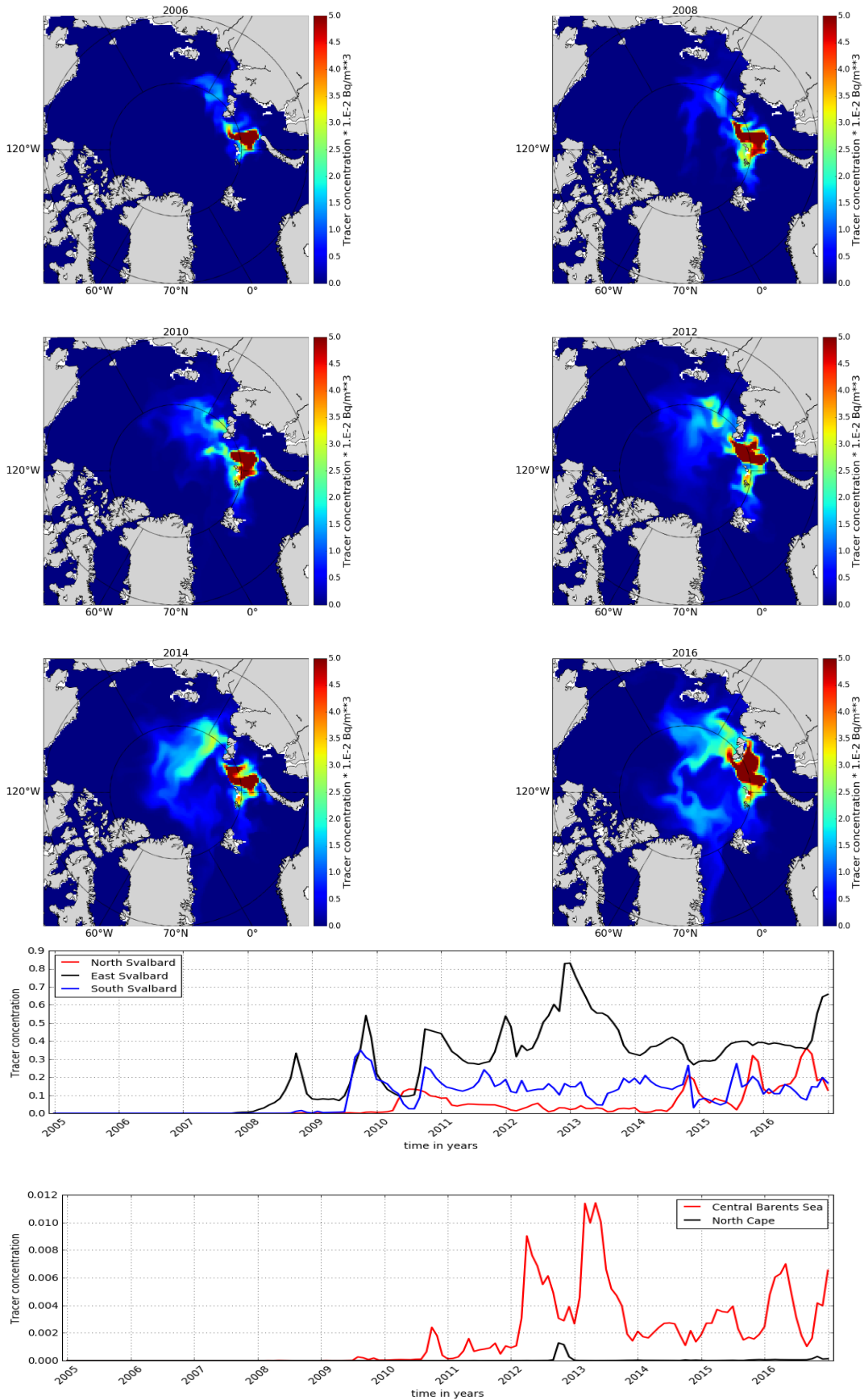
Figure 12: Continuous release of 1 TBq/yr North of Novaya Zemlya (start Jan 2005): concentration in the top 20m. Upper panels: dispersion patterns in December 2006-16; Bottom panels: timeseries at selected locations in Norwegian waters in 10^{-2} Bq/m^3 (see Fig 1).

2.4.3   June 2005 – May 2017, continuous release at the surface

To test how sensitive the levels of contamination are in the regions of Norwegian interest, with respect to seasonal circulation changes, experiments with a release in early summer were performed.

For the release from the location just North of the New Siberian Islands, the principal pattern of dispersion does not differ a lot from the case with a start of release in January (Fig. 13, upper panels). However, for the concentrations around Svalbard and in the Barents Sea (Fig. 13, bottom panels), d a peak of up to $2 \cdot 10^{-5}$ Bq/m^3 in early 2017 at the North Cape was observed, about twice the value that was reached here until the end of the January release experiment that finished in December 2016. It has been concluded that the circulation imposed an advection of contaminated water into that region that lasted a few months beyond December 2016. The summer release experiment captured the peak of that event in Spring 2017.

In a similar fashion about twice as high concentration at the North Cape occurs at the end of this early summer release experiment due to release North of Novaya Zemlya in June 2017 in comparison to the end of the January release experiment in December 2016 ($2 \cdot 10^{-4}$ Bq/m^3). Otherwise, the experiment with a release in early summer develops very similar in comparison to the January experiment (Fig. 14).
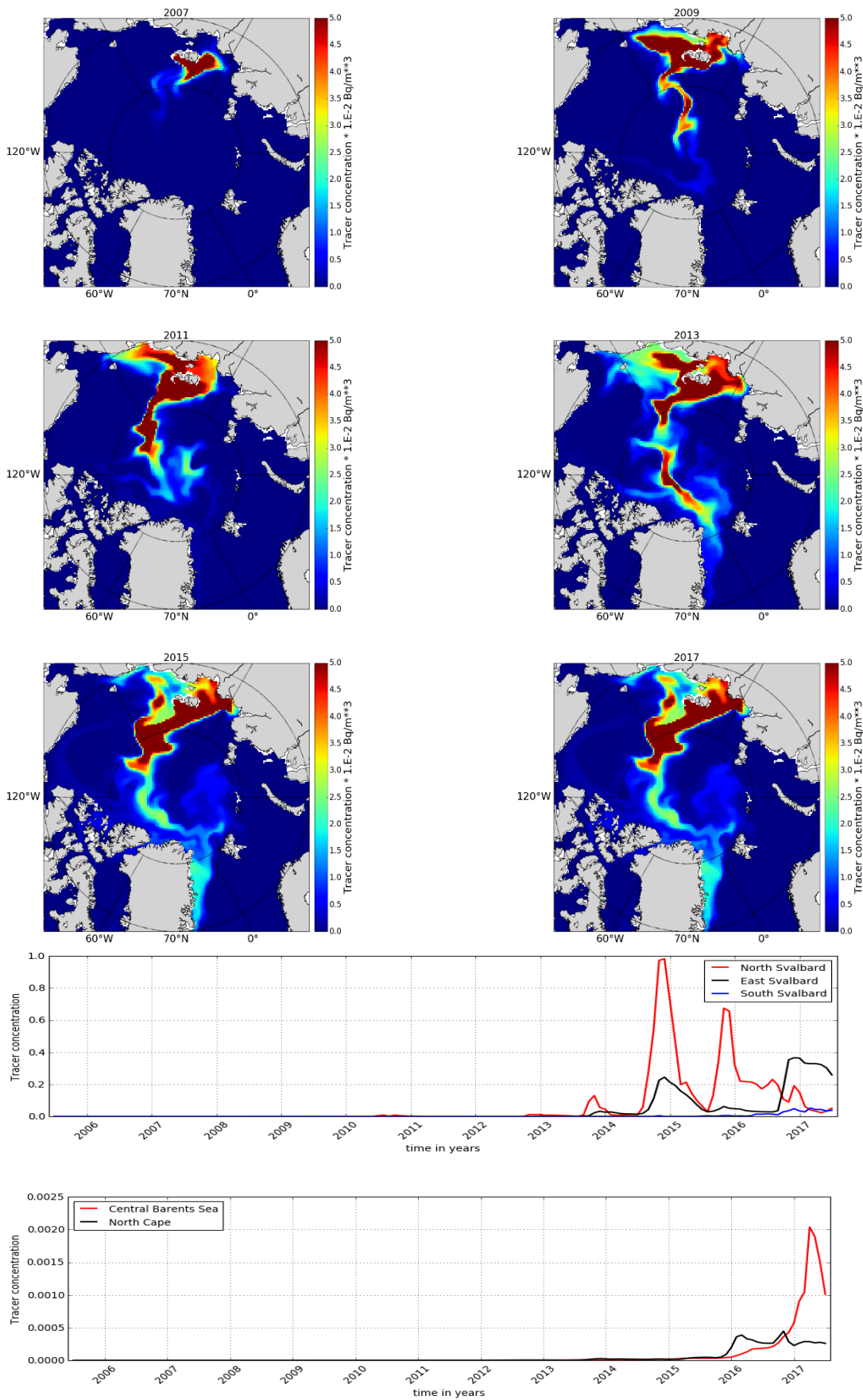
Figure 13: Cont. release of 1 TBq/yr North of the New Siberian Islands (start June 2005): concentration in the top 20m. Upper panels: dispersion patterns in June 2007-17; Bottom panels: timeseries at selected locations in Norwegian waters in 10^{-2} Bq/m^3 (see Fig 1).
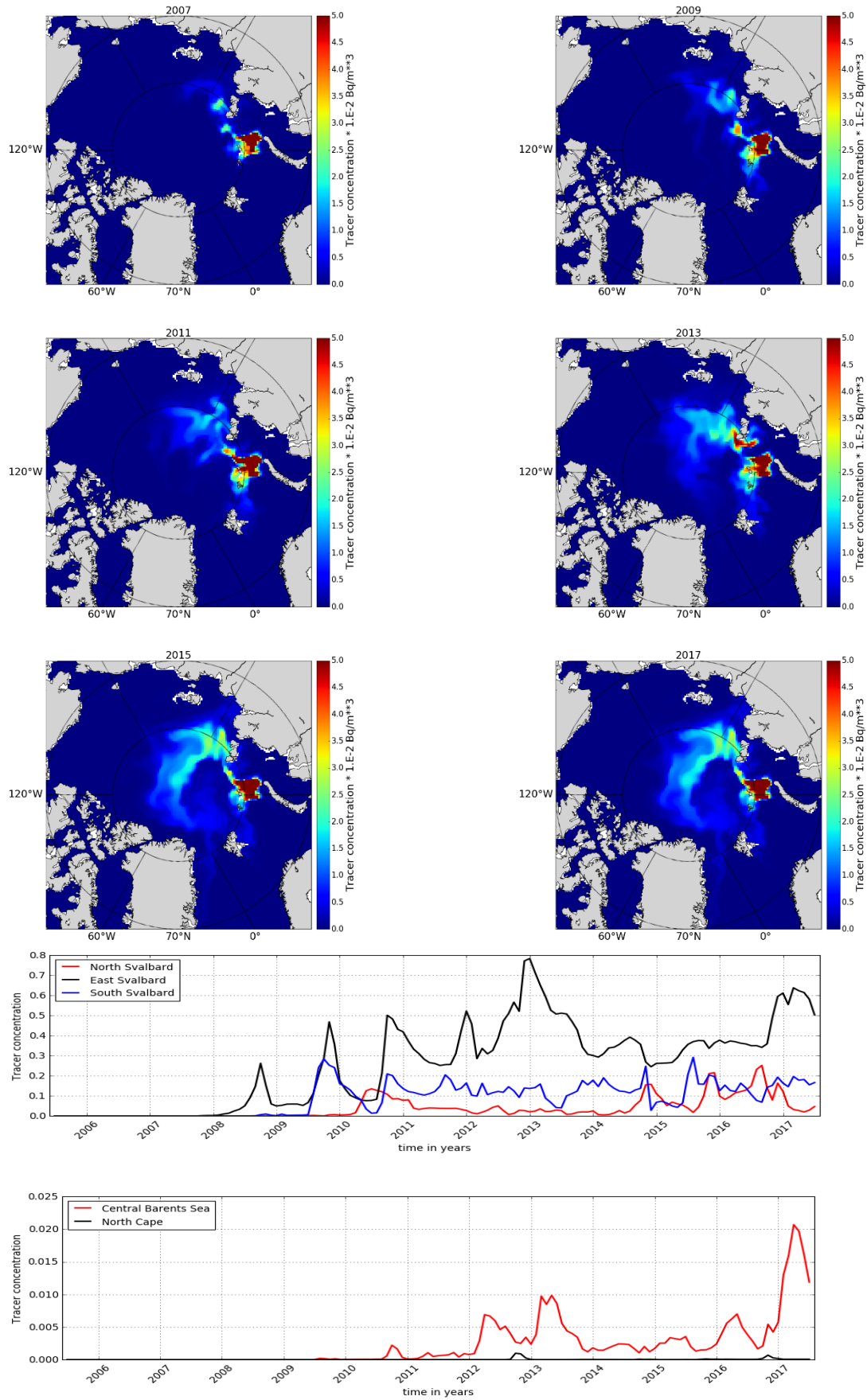
Figure 14: Continuous release of 1 TBq/yr North of Novaya Zemlya (start June 2005): concentration in the top 20m. Upper panels: dispersion patterns in June 2007-17; Bottom panels: timeseries at selected locations in Norwegian waters in 10⁻² Bq/m³ (see Fig 1).

2.4.4   Jan 1985 – December 1996, instantaneous release at the surface

The instantaneous release of 1PBq at the location off Pevek, on 1st January 1985, of course is subject to the same oceanic flow patterns as the continuous release experiment that started in that same month. However, concentrations in the basins are about an order of magnitude higher than for the 1TBq/year continuous release (Fig. 15, upper panels). On the shelf, in the vicinity of the release location, concentrations decrease with time as the area is flushed with uncontaminated water masses. In 1992, 8 years after release, the entire path of the Transpolar Drift with contamination levels well above 10 Bq/m3 reaching into Fram Strait is observable. Just north of the strait we see the intense recirculation events which were already obvious in the continuous release experiment taking place in that year. They are followed by three more such events in the years 1994, 1995 and 1997. Contamination levels reach 2-2.5 Bq/m^3 on the North and East coast of Svalbard (Fig. 15, bottom panels). A more intense inflow to the Barents Sea from the North in 1996 leads to concentrations in the central Barents Sea of about to 10^{-2} Bq/m^3.

Release from the location just North of Severnaya Zemlya shows characteristics of the signal dispersion different from the continuous release, despite the same flow pattern. The reason for this is the quick flushing of the source region. The isolated signal of contaminated water moves East and Northward before spreading along the Eurasian Basin in the early 1990s, 6 years after release (Fig. 16, upper panels). In the following years the signal is largely carried out of the Arctic proper with the East Greenland Current, while the rest is spreading inside the Arctic basin. In 1994 and the following years the signal moves into the Canadian Basin. This is a consequence of the increase of the Atlantic Water domain's extension to the East, following the high AO state described earlier. The maximum concentration on the Svalbard coast occurs in 1990 on the Northern shore with a peak of 6 Bq/m^3 and smaller peaks of 2-3 Bq/m^3 in the following years. Similarly, such peaks are observed at the East coast of Svalbard (Fig. 16, bottom panels). In the central Barents Sea maximum concentrations occur in 1996, just as was the case for the continuous release, but with about 0.1 Bq/m^3 the level is ten times higher.
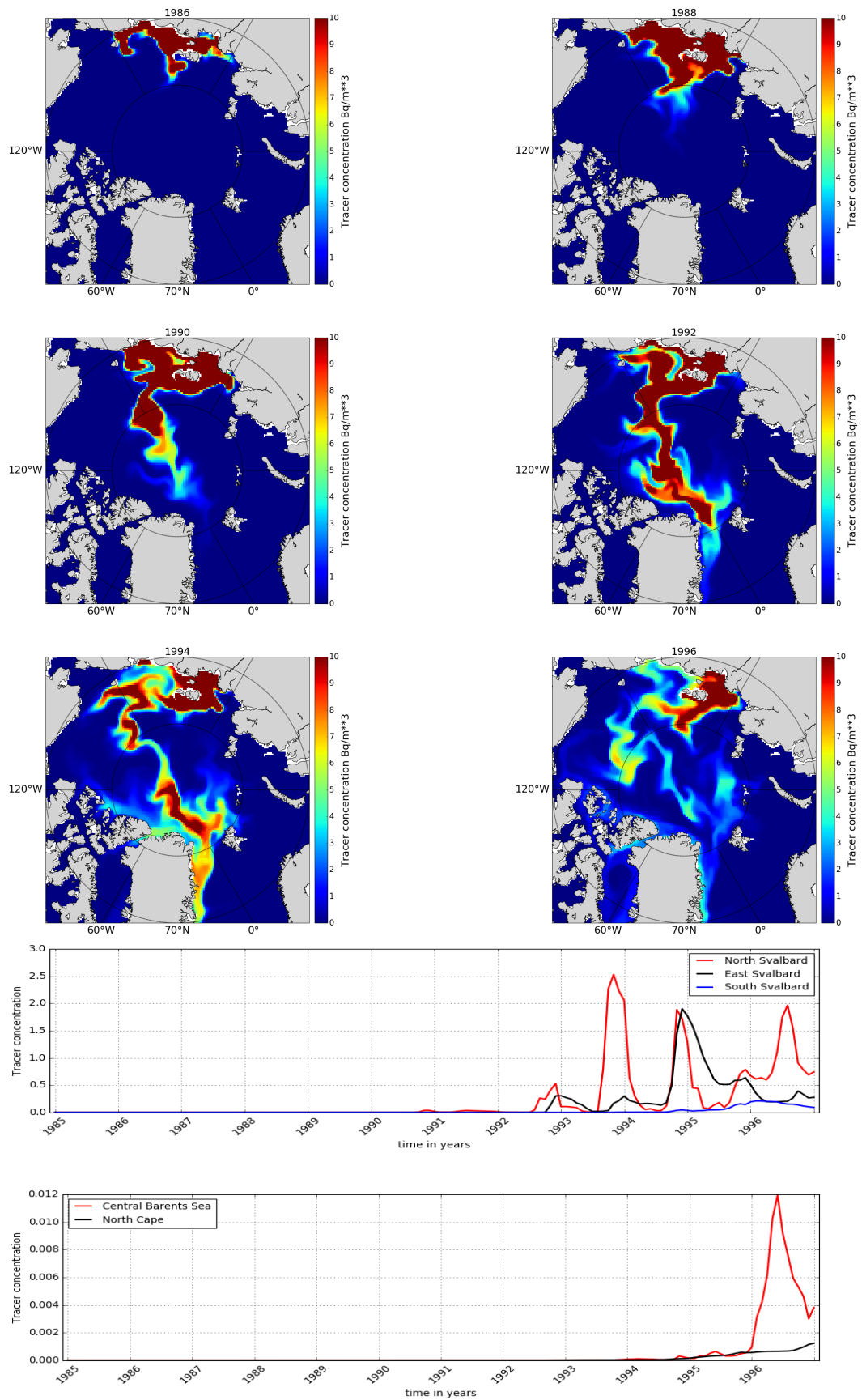
Figure 15: Instantaneous release of 1 PBq off Pevek (Jan 1st 1985): concentration in the top 20m. Upper panels: dispersion patterns in December 1986-96; Bottom panels: timeseries at selected locations in Norwegian waters in Bq/m³ (see Fig 1).
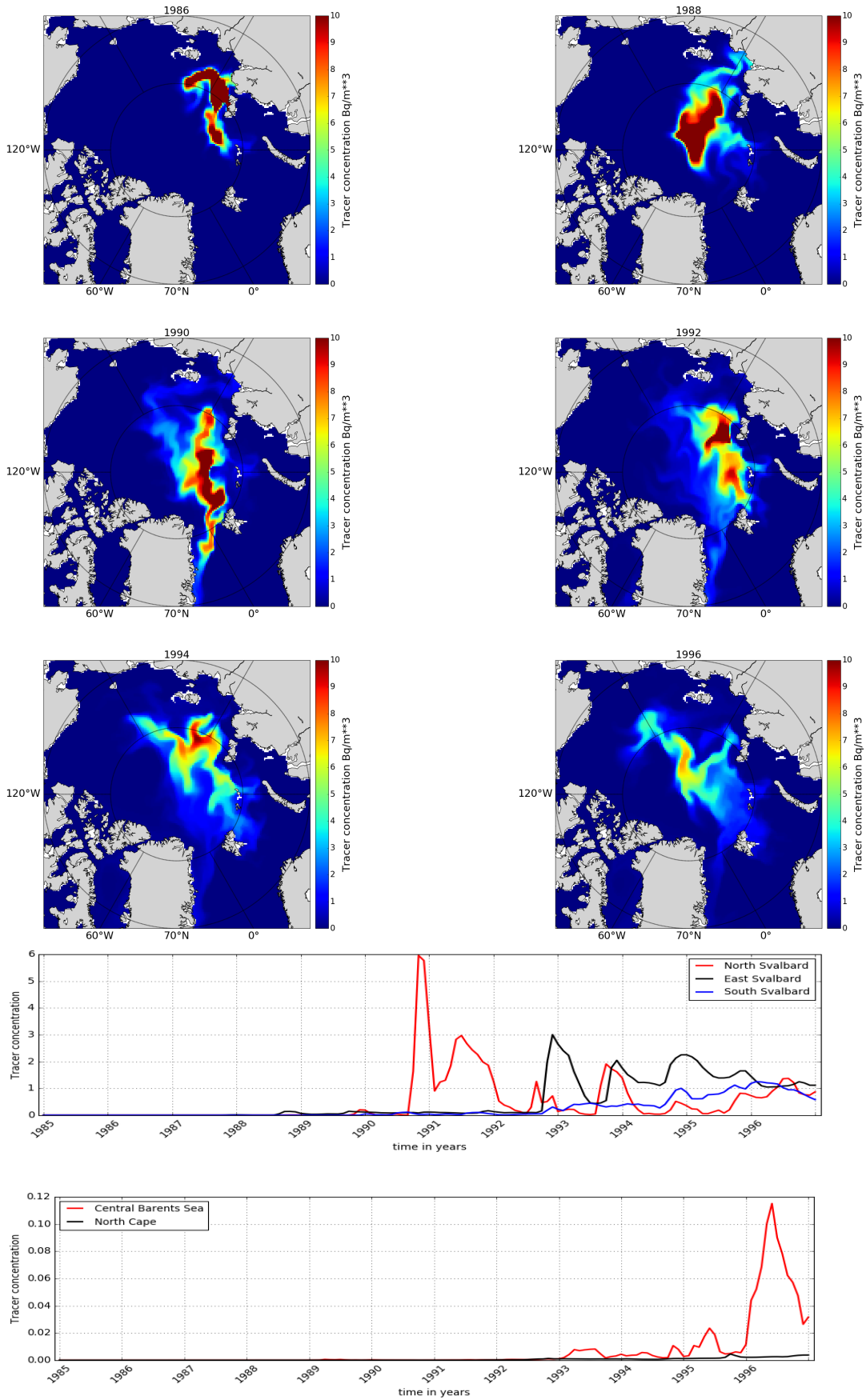
Figure 16: Instantaneous release of 1 PBq North of Severnaya Zemlya (Jan 1st 1985): concentration in the top 20m. Upper panels: dispersion patterns in December 1986-96; Bottom panels: timeseries at selected locations in Norwegian waters in Bq/m^3 (see Fig 1).

2.4.5   Jan 2005 – December 2016, instantaneous release at the surface

After the instantaneous release of 1PBq on 1st January 2005 at the location off Pevek, the contaminated water mass has a long residence time in the East Siberian Sea and in parts even moves Westward beyond the Chukchi Plateau to reach the coast of Alaska (2008, 4 years after release). In the same time period other parts of the signal spread into the Transpolar Drift towards Greenland and split, with one part moving into the East Greenland Current and the other part recirculating to the East into the Canadian Basin North of the Canadian Archipelago (Fig. 17, upper panels). Around Svalbard, maximum concentrations occur in 2014, 10 years after release, with 2.5 Bq/m^3 at the Northern coast (Fig. 17, bottom panels). The contamination in the central Barents Sea and at the North Cape show maximum contamination towards the end of the simulation with 3-4 10^{-3} Bq/m3.

Release from the location just North of Severnaya Zemlya on 1st January 2005, shows an instant advection to the Northeast, spreading in the Eastern Eurasian Basin for the first two years. Afterwards a quick dispersion of a large part of the contaminants along the Transpolar Drift and export to the Nordic Seas via the East Greenland Current occurs (Fig. 18, upper panels). By 2016, 12 years after the release, concentrations in the Western Eurasian Basin are well below 10 Bq/m^3. Concentrations around Svalbard exhibit a peak in 2014/15, 10 years after release, with values up to 4.5 Bq/m^3 at the Eastern coast (Fig. 18, bottom panels). In the central Barents Sea, the maximum occurs at the end of the integration period after 12 years, with concentrations up to 2 10^{-2} Bq/m^3 and at the North Cape just below 10^{-2} Bq/m^3.
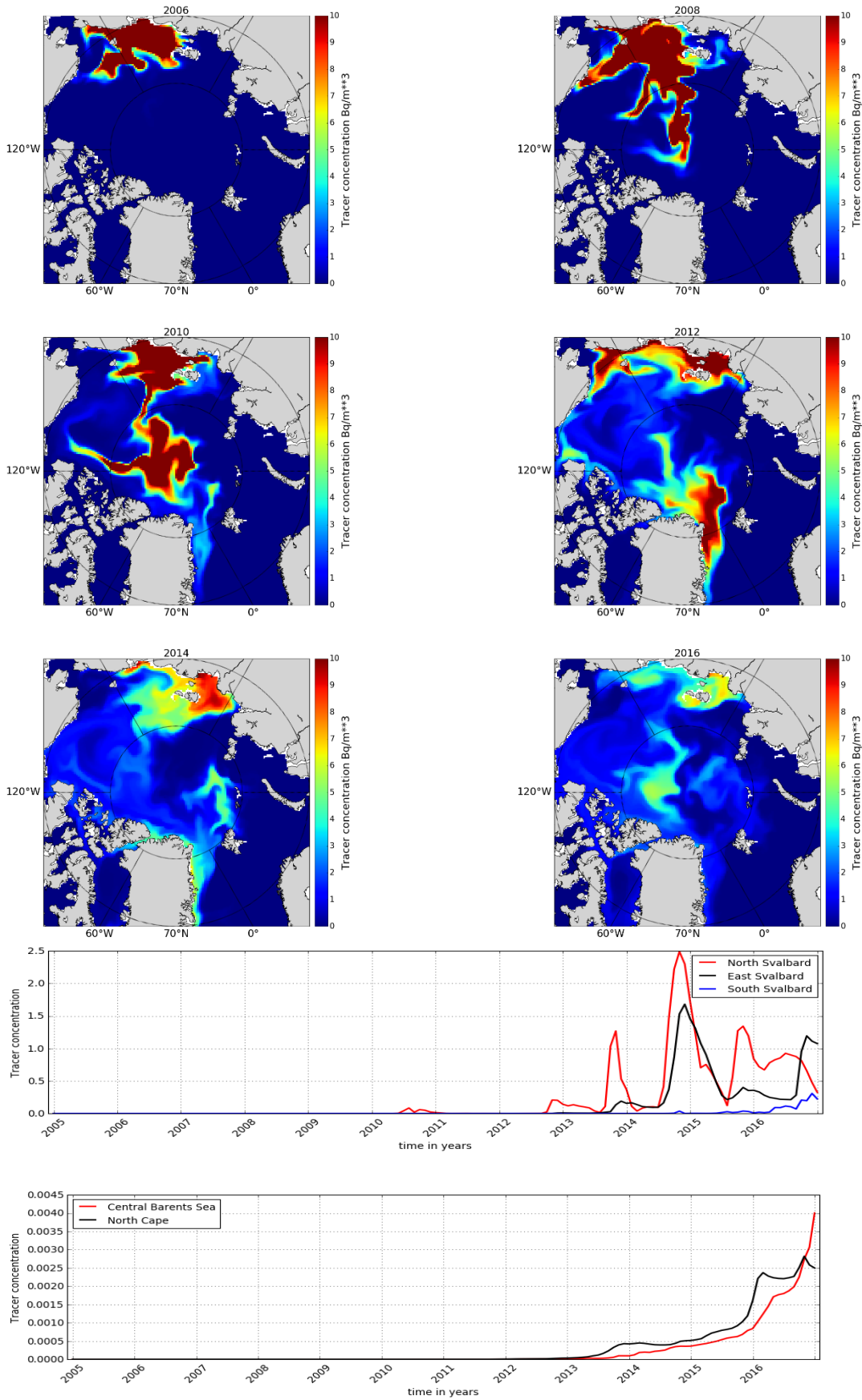
Figure 17: Instantaneous release of 1 PBq off Pevek (Jan 1st 2005): concentration in the top 20m. Upper panels: dispersion patterns in December 2006-16; Bottom panels: timeseries at selected locations in Norwegian waters in Bq/m³ (see Fig 1).

Figure 18: Instantaneous release of 1 PBq North of Severnaya Zemlya (Jan 1st 2005): concentration in the top 20m. Upper panels: dispersion patterns in December 2006-16; Bottom panels: timeseries at selected locations in Norwegian waters in Bq/m³ (see Fig 1).
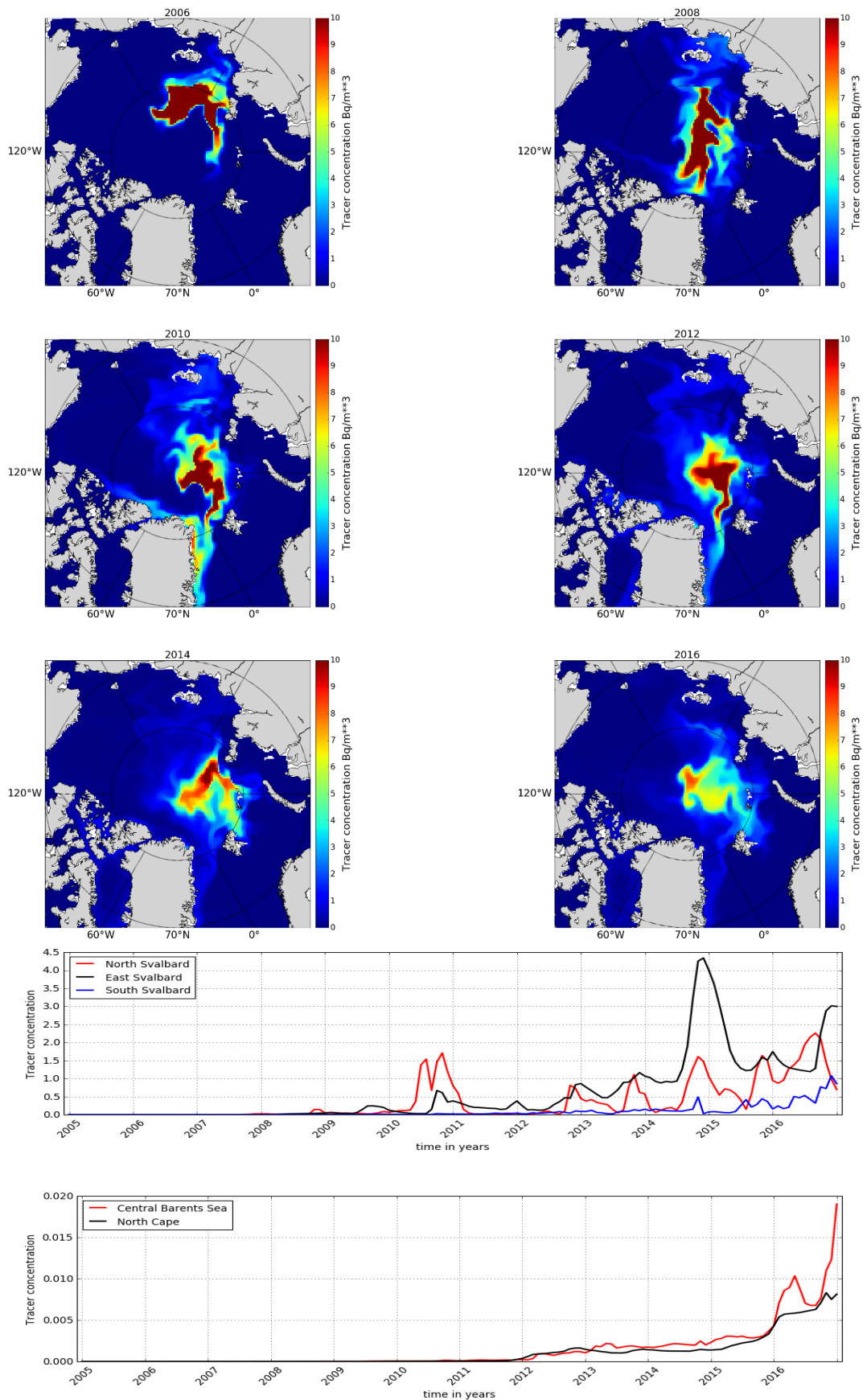
2.4.6   June 2005 – May 2017, instantaneous release at the surface

For the instantaneous release of 1PBq in summer on 1st June of 2005 at the location off Pevek (Fig. 19, upper panels), a very similar dispersion pattern as for the January release case for the same year is observed. As was observed in the comparison for continuous release in June versus in January, also here about twice the concentration levels are reached near the North Cape as was the case for the January release (1 10^{-2} Bq/m^3), comparing the respective ends of the experiments (May 2017 versus December 2016) (Fig. 19, bottom panels). Again, it is concluded that the summer release experiments which cover the first half of 2017 are able to capture the inflow of contaminated water from the North into the Barents Sea. This does occur independently from the actual release location but depends on the abundance of contaminated water in the Eurasian Basin in late 2016 and early 2017.

The relative highest concentrations in the regions of interest for Norway around Svalbard and in the central and southern Barents Sea (North Cape) occurred for releases from North of Severnaya Zemlya, from which a very direct flow occurs towards Svalbard with the Transpolar Drift. In the experiments performed here the maximum concentrations for a continuous release of 1 TBq/yr were 1-2 Bq/m^3 and for an instantaneous release of 1 PBq it was 5-10 Bq/m^3 on the coasts of Svalbard, respectively, with the release location North of Severnaya Zemlya.
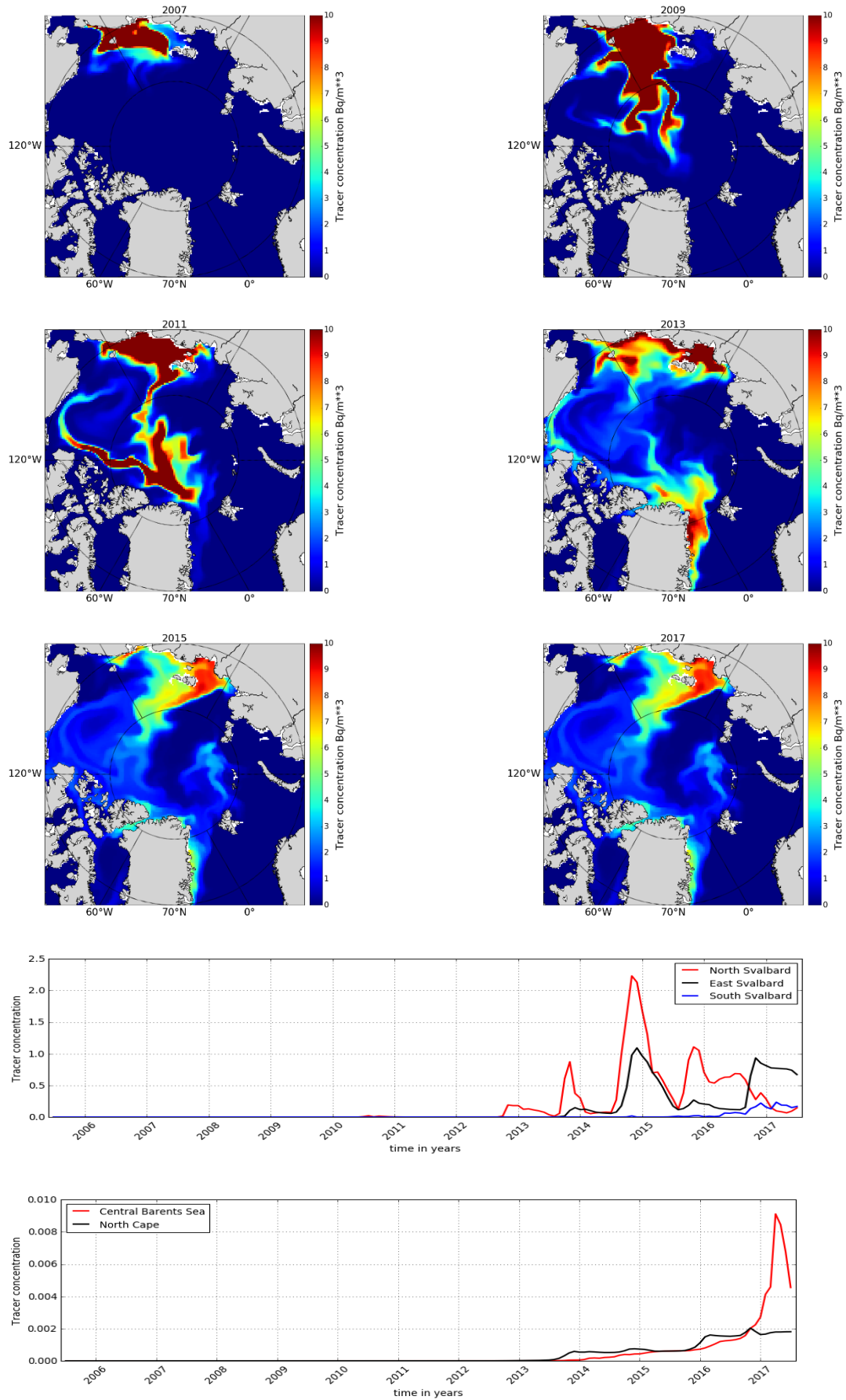
Figure 19: Instantaneous release of 1 PBq off Pevek (June 1st 2005): concentration in the top 20m. Upper panels: dispersion patterns in June 2007-17; Bottom panels: timeseries at selected locations in Norwegian waters in Bq/m³ (see Fig 1).

2.5   Marine dispersion – summary

A set of dispersion experiments for the potential continuous release of 1 TBq/yr or an instantaneous release of 1 PBq at the surface and at the bottom in 4 different locations of the FNPP: Pevek, North off the East Siberian Islands, North of Severnaya Zemlya, and North of Novaya Zemlya were performed. As expected there is a tendency for all release locations and time periods simulated, that the dispersion of the contaminant is directed to a large extent into the central Arctic Ocean. The major transport pathway to the main exit in Fram Strait is the Transpolar Drift. The experiments documented an advection time of about 8 years from Pevek to the coasts of Svalbard, and shorter for the release locations closer to Svalbard. The advection process is not continuous since the circulation patterns change in time. This may lead to subsequent pulses of increased contamination in the regions of interest to Norway even for instantaneous releases. Advection of the contaminant signal to the inner Barents Sea needs longer time, depending on the release location, and whether in periods of inflow to the Barents Sea from the North or from the East contaminated water masses are abundant in the Western Eurasian basin or the Northern Kara Sea, respectively.

The relative highest concentrations in the regions of interest for Norway around Svalbard and in the central and southern Barents Sea (North Cape) occurred for releases from North of Severnaya Zemlya, from which a very direct flow occurs towards Svalbard with the Transpolar Drift. In the experiments performed here the maximum concentrations for a continuous release of 1 TBq/yr were 1-2 10^{-2} Bq/m^3 and for an instantaneous release of 1 PBq it was 5-10 Bq/m^3 on the coasts of Svalbard, respectively, with the release location North of Severnaya Zemlya.

3 Atmospheric Dispersion

3.1 Model description

The atmospheric dispersion has been calculated using the Severe Nuclear Accident Programme (SNAP 2011), version 2.0.3-pevek (SNAP 2021). SNAP is a Lagrangian particle model for regional atmospheric transport. The dispersion is calculated using model-particles carrying a certain amount of radioactivity in Bq. Meteorological parameters such as wind speed, wind direction, turbulence and precipitation are used to calculate the transport and deposition. The meteorology used for driving the dispersion model was downloaded from the Copernicus Climate Change Service. The datasets ERA5 hourly data on pressure levels (Hersbach et al. 2018) and ERA5 hourly data on single levels (Hersbach et al. 2018) have been used for all days for the 16-year period from 2005-01-01 to 2020-12-31. The dataset contains meteorological parameters in a geographic grid in 0.25° degree horizontal resolution and 27 vertical pressure levels from 1000 hPa to 100 hPa. For transport between Pevek and Norway, only the northern hemisphere is of relevance. To achieve efficient dispersion calculations, the meteorology was interpolated to a 25 km polar-stereographic grid with 38 terrain-following eta-hybrid levels using the meteorological processor fimex, version 1.5.3 (Fimex 2020). SNAP transports particles using three-dimensional wind-directions and deposits particles either by dry- or wet-deposition (SNAP, 2011). SNAP parametrises diffusion depending on wind-speeds:

$$x'' = x' + r_x l$$

$$y'' = y' + r_y l$$

$$\eta'' = \eta' + r_\eta l_\eta$$

where x, y and η describe the particle's position, r is drawn from a uniform random number generator with a range between -0.5 and 0.5. The length-scale for turbulence motion is

$$l = a L^b$$

L is the horizontal wind velocity multiplied by timestep Δt, i.e. $L = \sqrt{(u^2+v^2)} * \Delta t$.

b = 0.875 and a = 0.5 within the atmospheric boundary and a = 0.25 above. The vertical diffusion is set by the parameter $l_\eta = 0.08$ within and $l_\eta = 0.001$ above the atmospheric boundary layer.

SNAP was run for the hemispheric domain of 9600 x 9600 km² centered at the North pole covering the domain as shown in Figure 20. Twice on each day, at 00 and 12, a SNAP-run was started and modelled the dispersion of a hypothetical accident for 14 days. Output from the model was written every 24h. Low altitude emissions usually have a short atmospheric lifetime, e.g. 2-4 days and the long dispersion runtime ensured 99% of all emissions were either deposited or had left the domain at the end of the run.
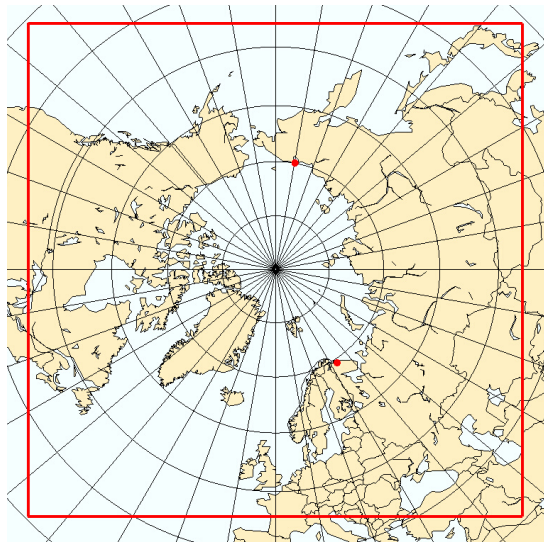
Figure 20: Map showing the domain where SNAP modelling was undertaken.

3.2 Source-term specification for dispersion calculations
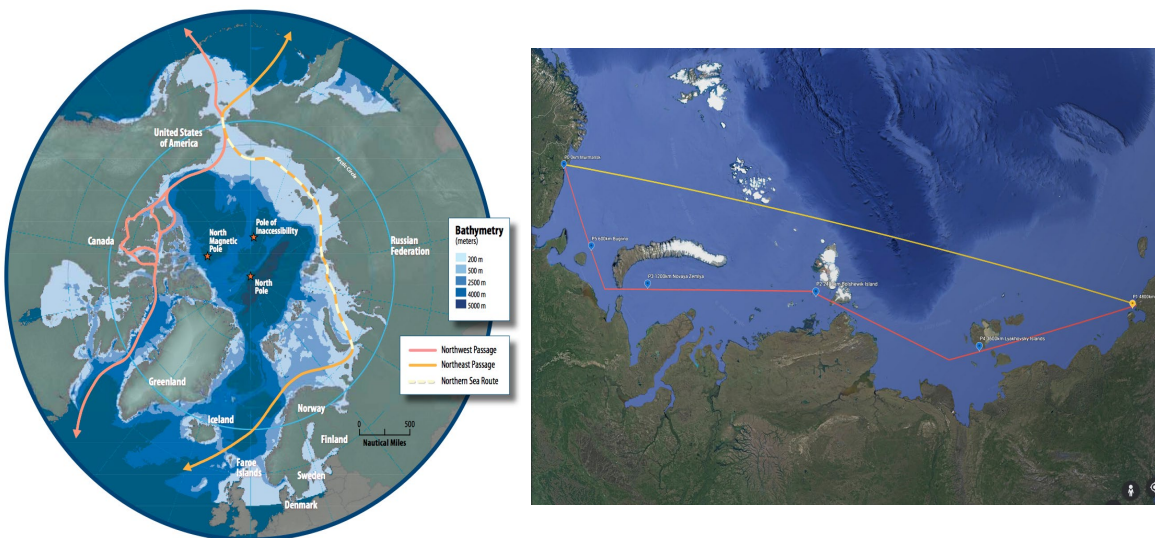

Figure 21: Map of the Northern Sea Route of the North-East passage according to Wikipedia and 6 positions selected for calculations on a hypothetical route roughly following the North-East passage between Pevek and Murmansk.

Since the hypothetical accident used as a release scenario in this study might occur at any point during the transport of the vessel between Pevek and Murmansk, a route roughly following the North-East passage was selected and example-locations where selected such that the first points were 600 km, 1200 km, 2400 km and 3600 km from Murmansk. In addition, Murmansk and Pevek, having a distance of ~4800 km, were used as possible emission locations. These locations can be seen in Figure 21 and are listed in Table 2.

Table 2: Assumed locations where SNAP was calculated

	Name	Distance	Latitude	Longitude
P0	Murmansk	0 km	69.38	33.65
P1	Pevek	4800 km	69.95	169.79
P2	Bolshewik Island	2400 km	78.05	95.26
P3	Novaya Zemlya	1200 km	72.03	61.04
P4	Lyakhovsky Islands	3600 km	74.54	137.83
P5	Bugrino	600 km	69.92	49.07

The total release to the atmosphere consisted of 1 PBq of radionuclides, corresponding approximately to 1 % release of the inventory of 4 loads of spent nuclear fuels. For simplicity all radionuclides were transported as ^{137}Cs, i.e. as aerosol particles with radius of 0.55 μm and density of 2.3 g/cm³. The release was uniformly distributed and assumed to last 12 hours, such that with diurnally restarting snap-runs, the complete 16-year archive was covered. Since a conventional fire was assumed, the emissions were released as a 50 m diameter column of 150 m height.

3.3 Methodology

Running SNAP twice each day for 16 years and 6 release positions results in 70128 dispersion runs. These runs were then analyzed statistically. To assess the impact to Norwegian territory, deposition above the minimum threshold of 10 Bq/m² was considered. Both the maximum deposition on any location, and the total deposition above the threshold on all the Norwegian territory was investigated. For this a "land-mask" of Norway, including the islands of Svalbard, Hopen and Jan Mayen, was applied to the map and dispersion runs. Quantiles of the total depositions above the threshold are shown in Figure 22, showing that an accident in Murmansk will in 37 % of all meteorological cases result in no deposition above the threshold value in Norway, i.e., in 63 % of all meteorological cases, Norway will be affected. For Pevek, only 4 % of all cases affect Norway. In increasing order of distance from Murmansk the percentage of cases affecting Norway are: Bugrino (43 %, 600 km), Novaya Zemlya (35 %, 1200 km), Bolshewik Island (31 %, 2400 km), Lyakhovsky Islands (15 %).
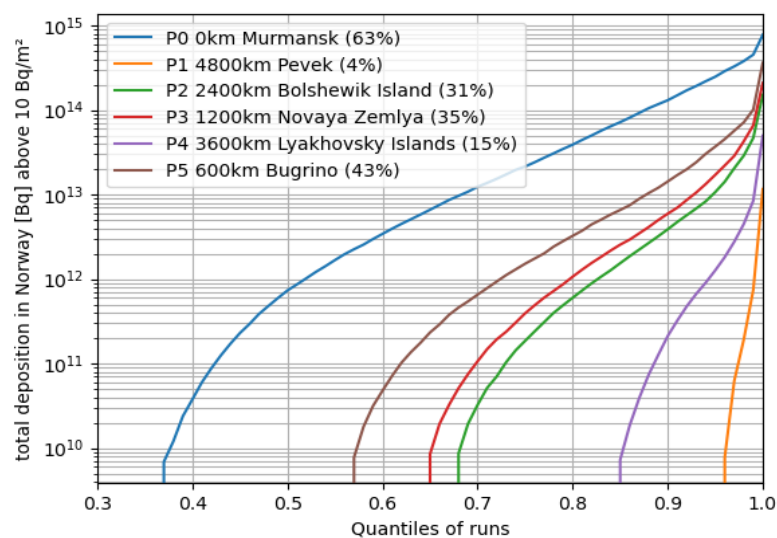

Figure 22: Quantiles of total depositions in grid-cells with at least 10 Bq/m² deposition on Norwegian territory

The maximum deposition per grid-cells versus the quantiles of the different meteorological cases is plotted in Figure 23. The intersection with the 10 Bq/m² threshold indicates again the same percentage of runs affecting Norway. It is interesting to note that the lines for Novaya Zemlya (red) with a shipping distance to Murmansk of ~1200 km and for Bolshewik Island (dark green) with double this distance from Murmansk are close in total deposition to Norwegian territories. Besides the case of an accident during transport, the floating NPP might have a nuclear accident, but with approximately ¼ of the emissions since it only contains 1 load of nuclear fuel. In this case, the meteorological probability of depositing at least 10 Bq/m² anywhere in Norway is only 0.9 %.

The behavior of distance from a release location to maximum deposition is plotted in Figure 24. For all 6 positions, the curve indicates similar behavior in the release for distances further than 100 km from the source. The Nordic Guideline threshold for slightly contaminated areas of 100 kBq/m² (Flaggbok 2014) is no longer exceeded outside a 500 km range in the downwind direction of the accident. Contaminated areas (>1000 kBq/m²) exist only within ~20 km, but the model resolution does not resolve such short distances well. Only with a release from Murmansk would depositions above 100 kBq/m² be expected, while an accident with a seaway distance of more than 2000 km from Murmansk will not exceed 10 kBq/m² in Norway.
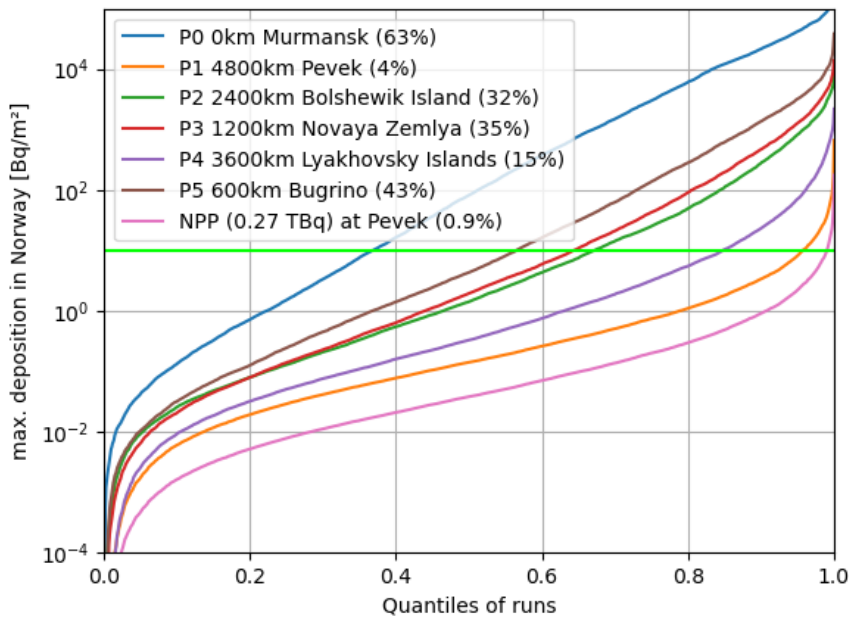

Figure 23: Quantiles of maximum depositions, the minimum threshold of 10 Bq/m² and the percentage of runs above the threshold in brackets. The 6 positions with a release of 1 PBq and the NPP in Pevek with 0.27 TBq are plotted
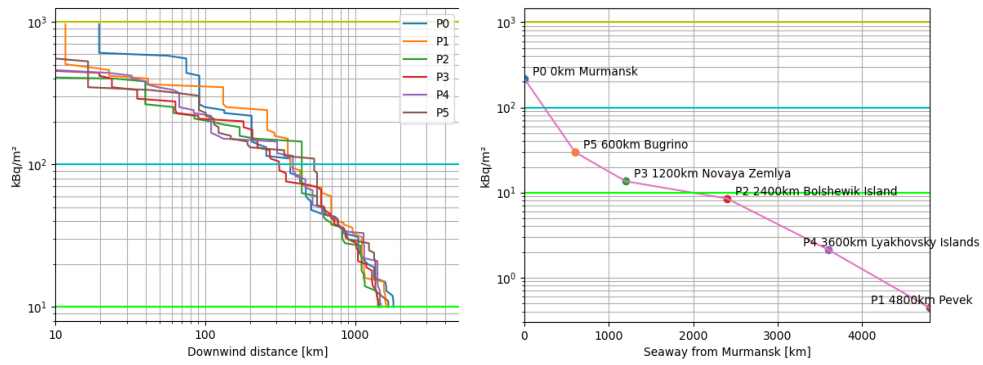
Figure 24: Maximum depositions found downwind (left) for the 6 positions and max. deposition in Norway dependent on distance (right) depending on the seaway to Murmansk of the 6 positions. The horizontal lines represent threshold values for slightly contaminated (cyan) and contaminated (yellow) areas

The probability of reaching a certain grid-cell rather than any point in Norway is plotted in Figure 25. The probabilities for each grid-cell in Norway is of course much lower than the combined probability in any cell in Norway. The closer grid-cells are more often affected than those further away. Therefore, for most releases, except Murmansk, it is more likely to reach Svalbard than the Norwegian-Russian border.
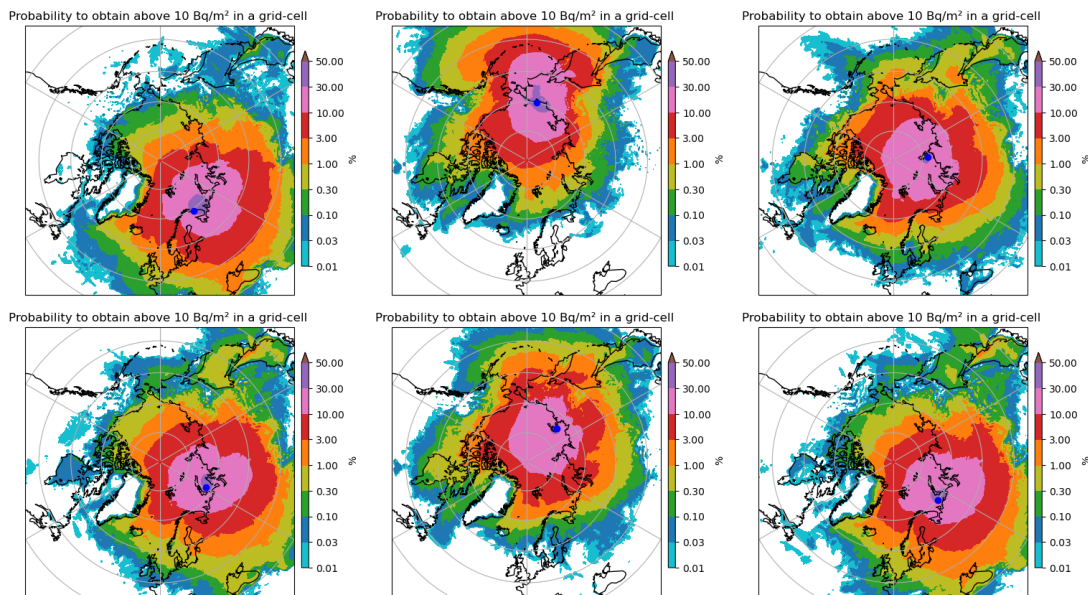

Figure 25: Maps showing probability of more than 10 Bq/m² deposition in a grid cell

The dispersion results giving most deposition in Norway are shown in Figure 26 to Figure 31. For emissions from Murmansk and Bugrino in Figure 26 and Figure 31, strong winds are not necessary, but the wind needs to be oriented in the direction of northern Norway with heavy deposition, i.e., precipitation in Finnmark. Deposition exceeding the minimum threshold may occur in Troms or Svalbard. As soon as the seaway distance to Murmansk is greater than 2000 km, i.e., Pevek, Bolshewik Island and Lyakhovsky Islands in Figure27, Figure 28 and Figure 30, strong wind towards Svalbard are required. For Novaya Zemlya in Figure 29 cases with strong deposition exist for Northern Norway and Svalbard, or even affecting both areas.
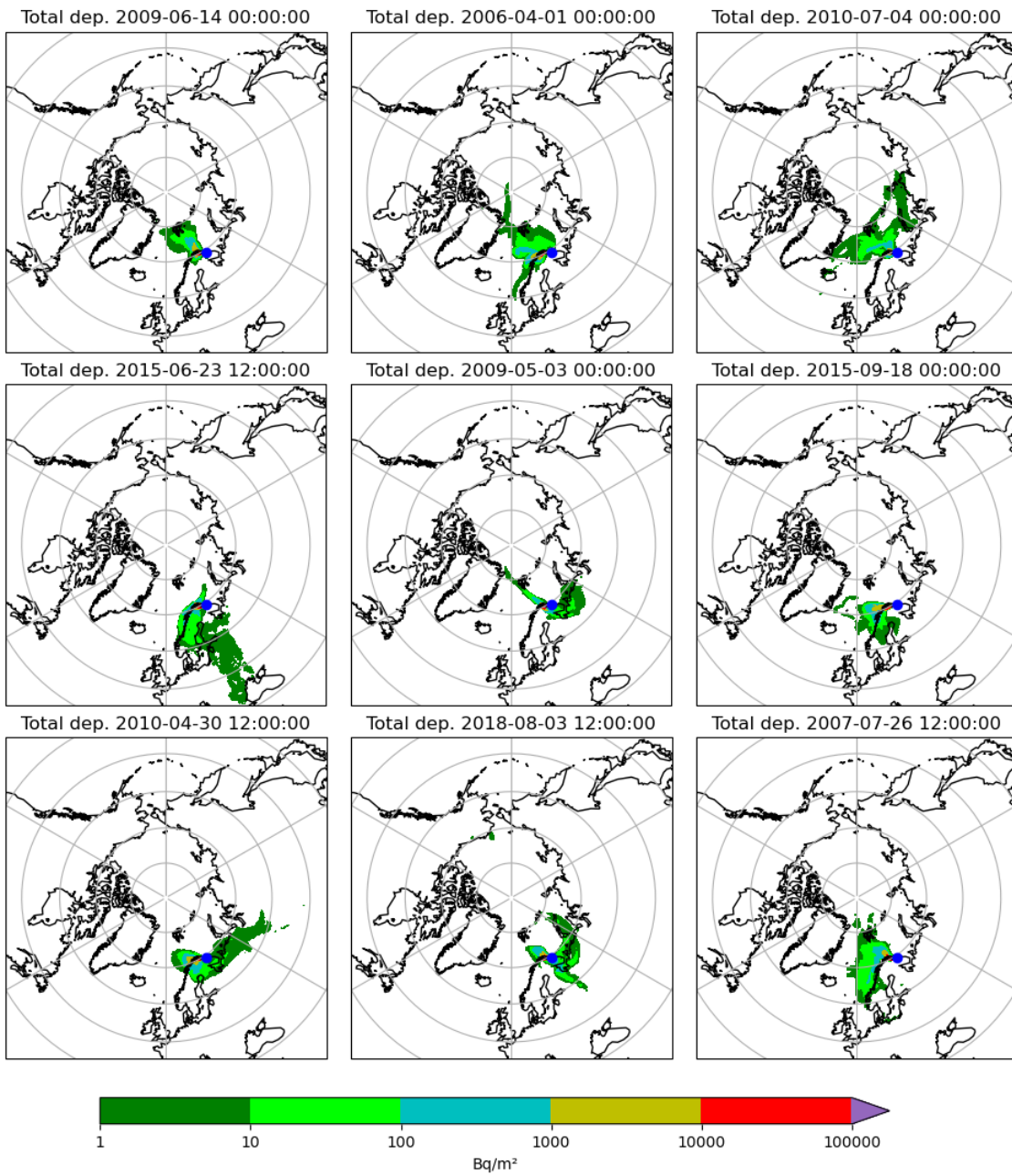
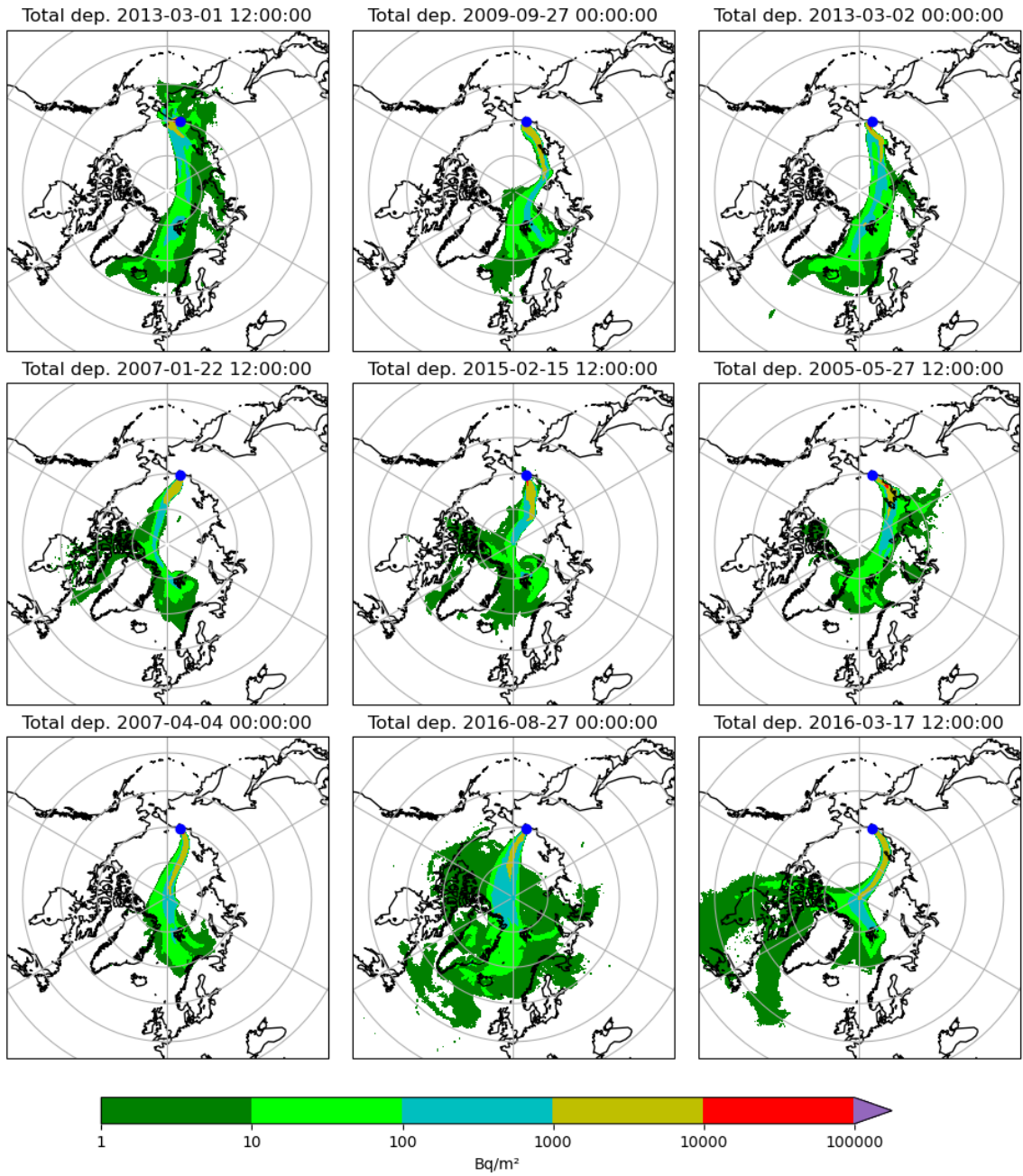**Figure 26:** Maps showing cases with largest total deposition in Norway starting from Murmansk.

Figure 27: Maps showing cases with largest total deposition in Norway starting from Pevek.
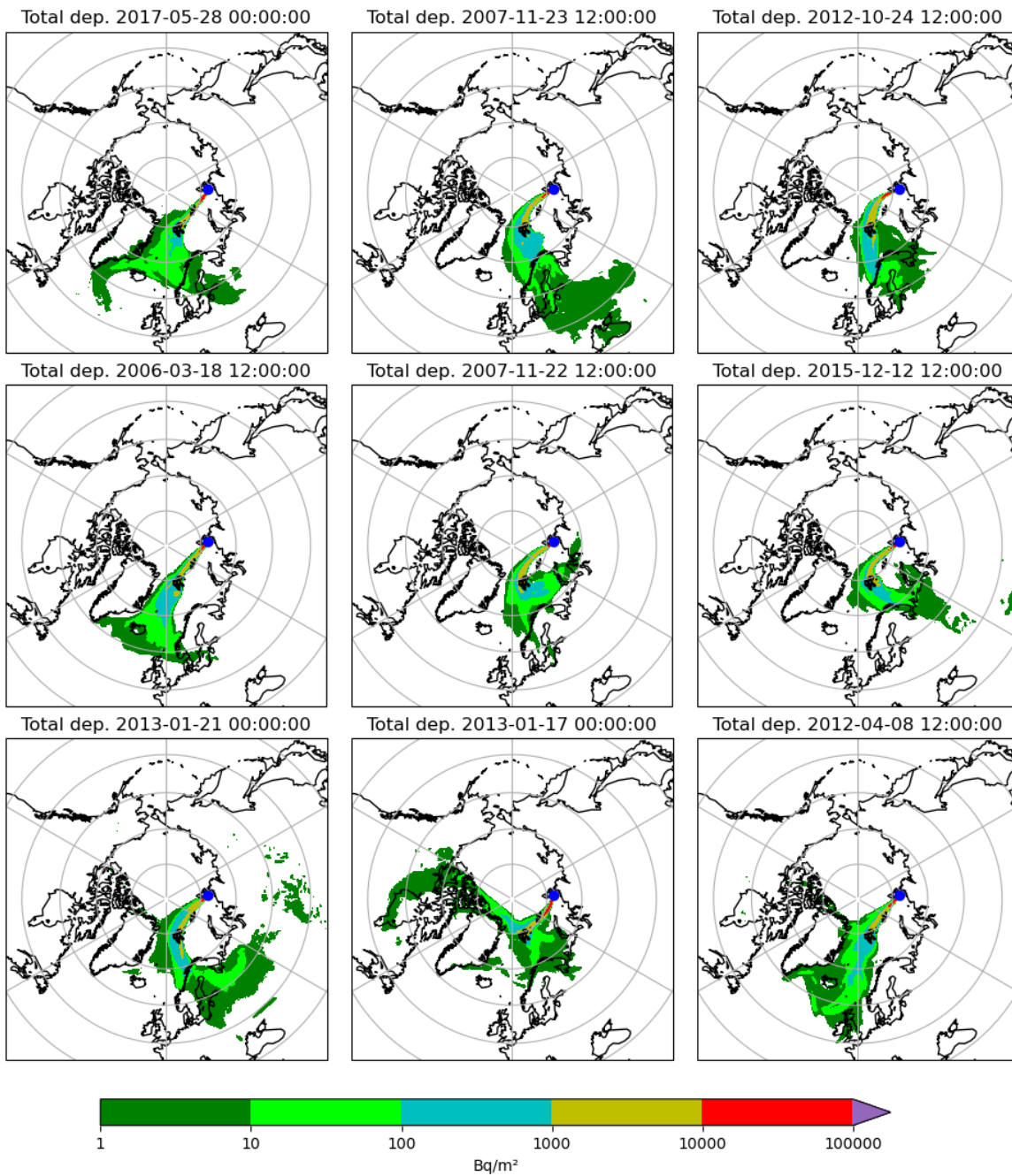
Figure 28: Maps showing cases with largest total deposition in Norway starting from Bolshewik Island.
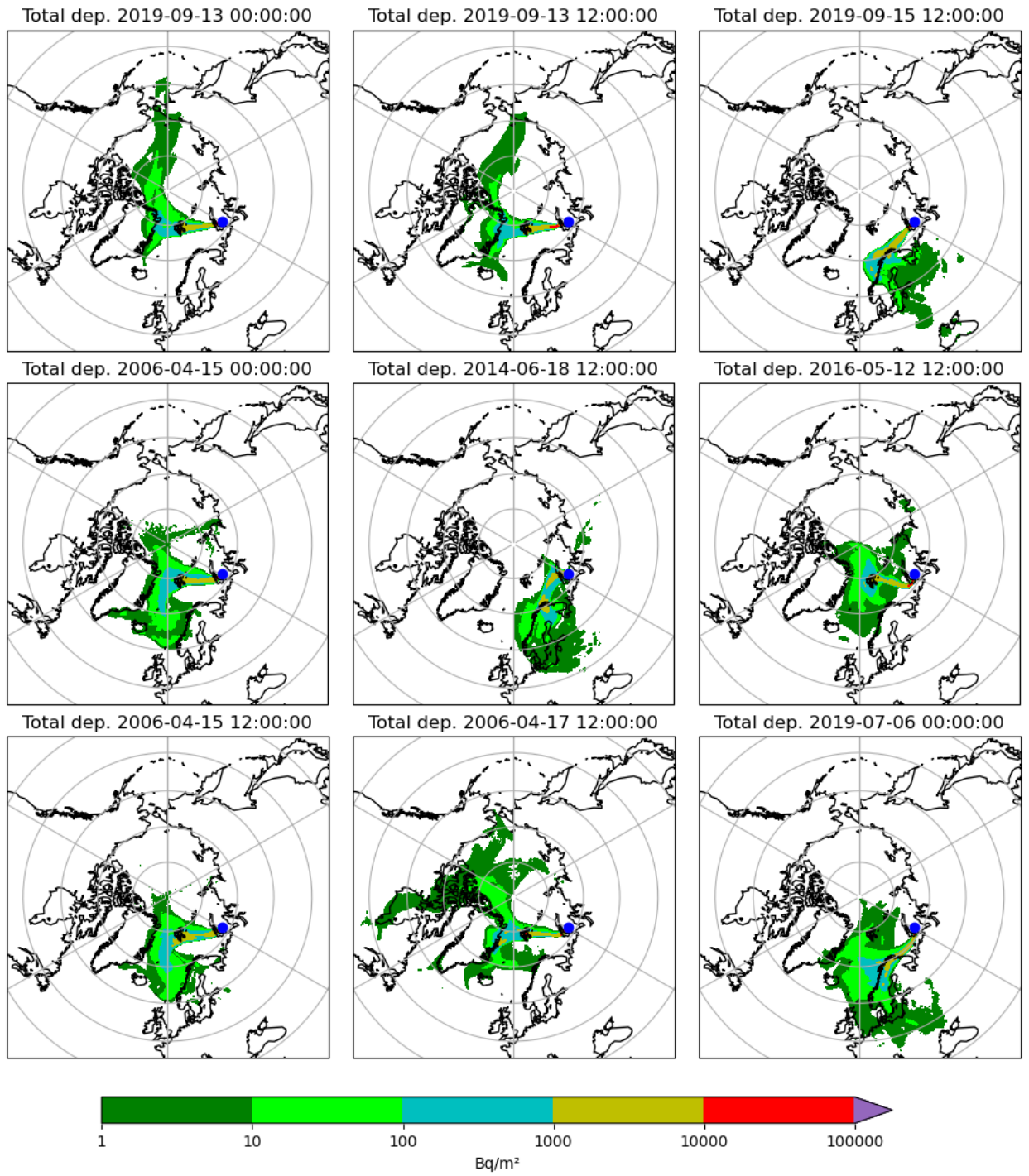
Figure 29: Maps showing cases with largest total deposition in Norway starting from Novaya Zemlya.
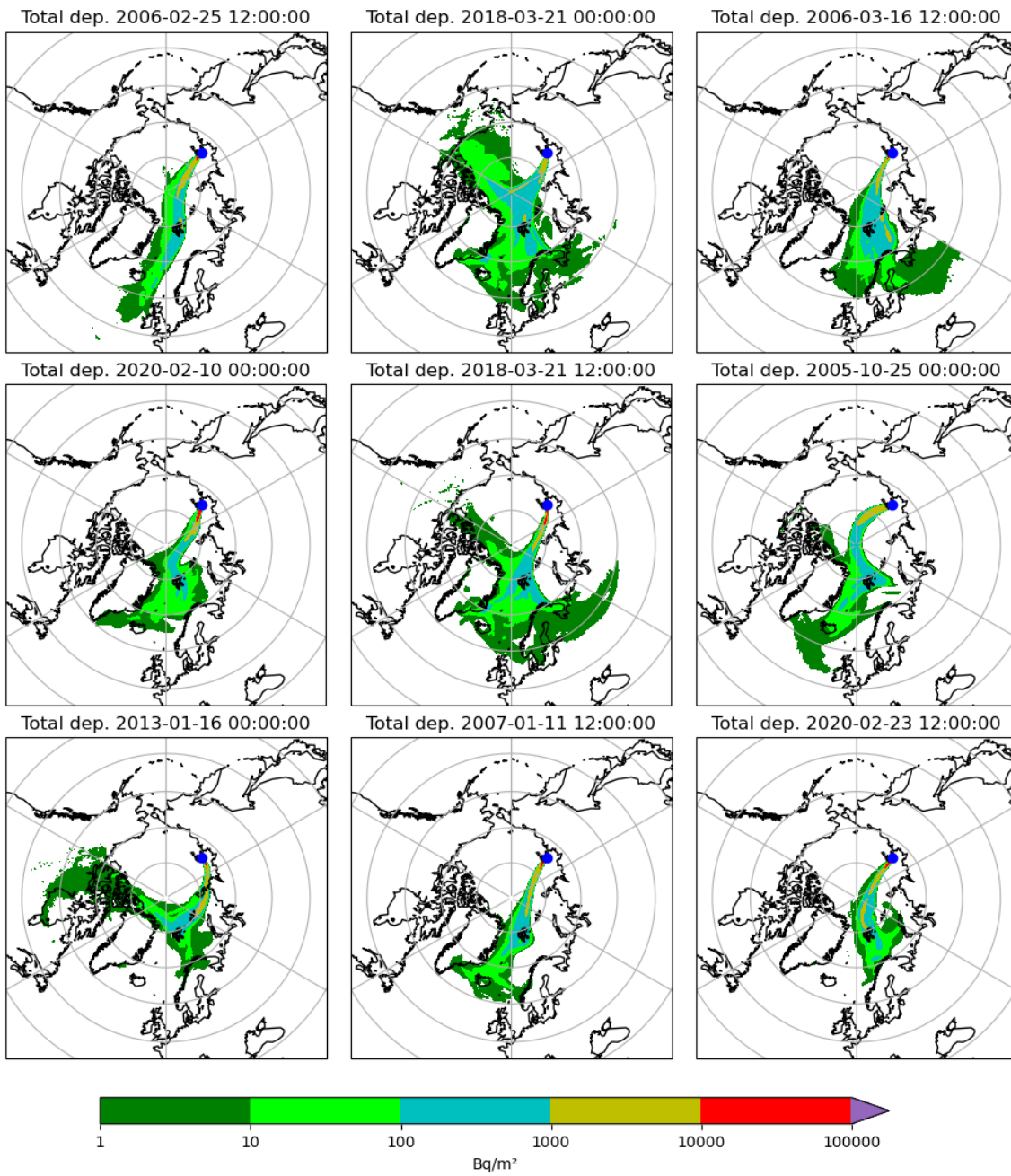
Figure 30: Maps showing cases with largest total deposition in Norway starting from Lyakhovsky Islands.
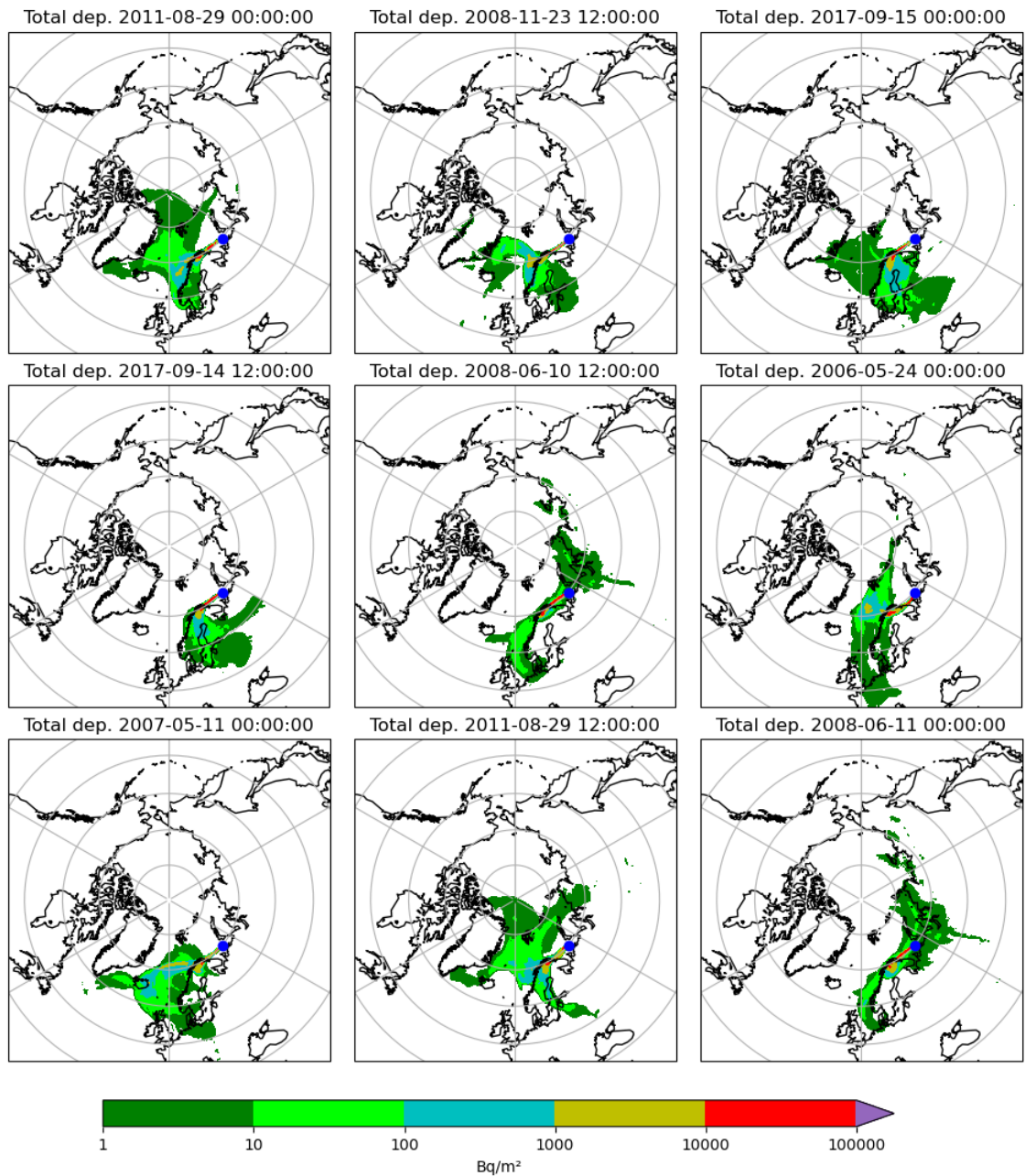
Figure 31: Maps showing cases with largest total deposition in Norway starting from Bugrino.

3.4 Time of arrival

The minimal time of arrival at each grid-cell for the 6 scenario locations can be seen in Figure 32. The time-resolution is limited by the output-resolution of 24 hours. From the furthest release location of Pevek, northern Norway can be reached within 3-4 days, while the plume may reach Svalbard after 2 days. These times of arrivals additionally is approximately similar for Lyakhovsky Islands. For all other cases, northern Norway and Svalbard can be reached within 24 hours.

Figure 32: Maps showing time of arrival of the radioactive plume from the 6 positions (clockwise from top left: Murmansk, Pevek, Bolshewik Island, Bugrino, Lyakhovsky Islands, Novaya Zemlya).
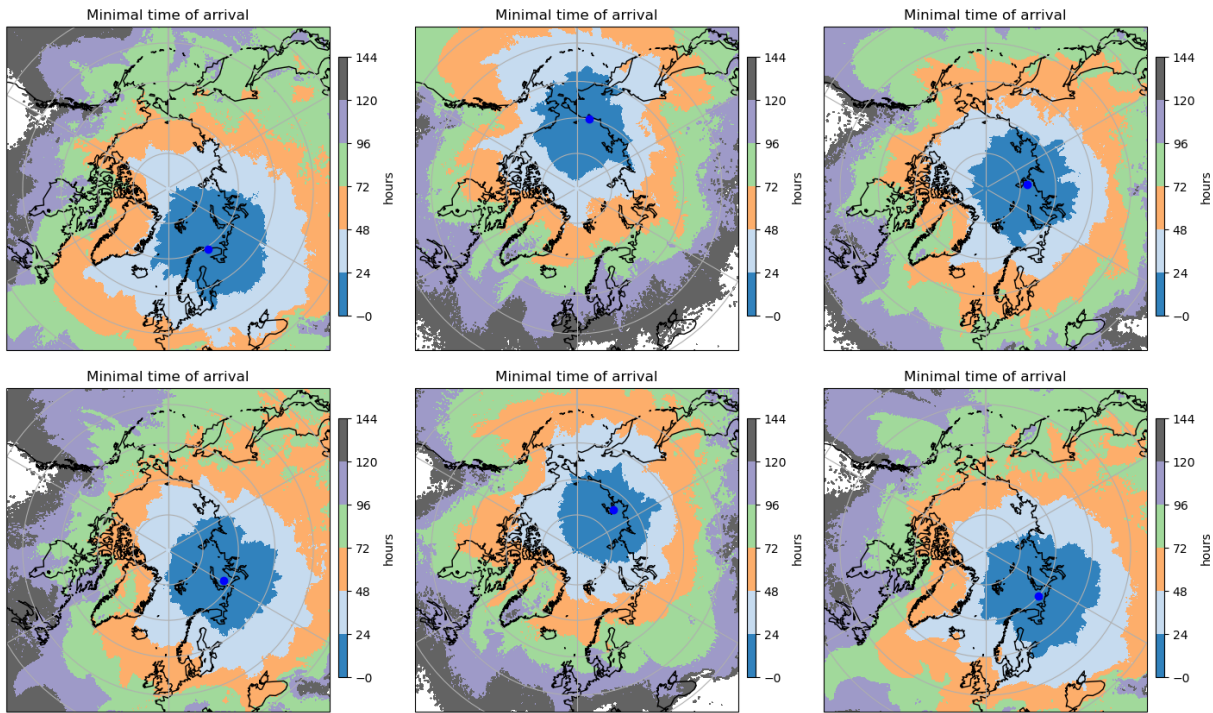
3.5   Atmospheric dispersion – summary

Analyzing the statistical properties for meteorological transport to Norway following a hypothetical accident on a FNPP vessel emitting 1 PBq of ^{137}Cs for 6 different locations between Murmansk and Pevek shows that the probability for deposition of more than 10 Bq/m^2 in Norway varies between 4 % from Pevek to 63 % in Murmansk. An accident on the NPP located in Pevek with emission of only 0.27 PBq will still have a 0.9 % likelihood of reaching Norway. For accident locations between Murmansk and Novaya Zemlya, Finnmark is the most affected area, while between Novaya Zemlya and Pevek, the worst case tends towards Svalbard. A threshold-value of 10 kBq/m^2 in Norway was not found to be exceeded as long as the release point exceeded a distance to Murmansk of about 2000 km, a distance close to Bolshewik Island.

Transport of the radioactive plume is swift in the worst case. From Pevek the atmospheric transport may take slightly more than 3 days to Finnmark and only 2 days to Svalbard. For closer locations, transport to Svalbard or northern mainland Norway may be less than 24 hours.

4   Conclusions

The results from marine dispersion experiments for the potential continuous release of 1 TBq/yr or an instantaneous release of 1 PBq into surface water and at the sea bottom in 4 different potential locations of the FNPP (Pevek, North off the East Siberian Islands, North of Severnaya Zemlya, and North of Novaya Zemlya) showed a tendency for all release locations and time periods simulated, that the dispersion of the contaminant is directed mostly into the central Arctic Ocean. The major transport pathway to the main exit point in Fram Strait is the Transpolar Drift. The experiments revealed an advection time of about 8 years from Pevek to the coast of Svalbard, and shorter times of arrival for the release locations closer to Svalbard. The advection process is not continuous since the circulation patterns change with time. This may lead to subsequent pulses of increased contamination in the regions of interest to Norway even for instantaneous releases. Advection of the contaminant to the inner Barents Sea takes longer time, dependent on the release location, and whether the release occurs in periods of inflow to the Barents Sea from the North or from the East.

The relative highest concentrations in the regions of interest for Norway around Svalbard and in the central and southern Barents Sea (North Cape) occurred for releases from North of Severnaya Zemlya, from which a very direct flow can occur towards Svalbard with the Transpolar Drift. From such locations (North of Severnaya Zemlya), the maximum concentrations for a continuous release of 1 TBq/yr were 1-2 10^{-2} Bq/m^3 and for an instantaneous release of 1 PBq it was 5-10 Bq/m^3 off the coast of Svalbard, respectively.

The air dispersion experiments studied the statistical properties of meteorological transport to Norway following a hypothetical accident on a FNPP vessel emitting 1 PBq of ^{137}Cs for 6 different locations between Murmansk and Pevek. Results show that the probability for deposition of more than 10 Bq/m^2 in Norway varies between 4 % from a release in Pevek to 63 % for a Murmansk release. An accident on the FNPP located in Pevek with an emission of only 0.27 PBq will still have a 0.9 % likelihood of reaching Norway. For accident locations between Murmansk and Novaya Zemlya, Finnmark is the most affected area, while between Novaya Zemlya and Pevek, the worst case tends towards Svalbard. A threshold-value of 10 kBq/m^2 in Norway was not found to be exceeded as long as the release point exceeded a distance to Murmansk of about 2000 km, a distance close to Bolshewik Island.

Transport of the radioactive plume in air is swift in the worst case. From Pevek the atmospheric transport may take slightly more than 3 days to Finnmark and only 2 days to Svalbard. For closer locations, transport to Svalbard or northern mainland Norway may be less than 24 hours.

5   References

AMAP 1998. AMAP assessment report: Arctic pollution issues. Arctic Monitoring and Assessment Programme (AMAP), Oslo, Norway. Xii+859 pp.

Bjo¨rk G, So¨derkvist S, Winsor P, Nikolopoulos A, Steele M. Partial return of the cold halocline layer to the Amundsen Basin of the Arctic Ocean: implications for sea ice mass balance. Geophys Res Lett 2002.

Brown, J. , Hosseini, A. , Karcher, M. , Kauker, F. , Dowdall, M. , Schnur, R. and Strand, P. (2016): Derivation of risk indices and analysis of variablility for the management of incidents involving the transport of nuclear materials in the Northern Seas , Journal of Environmental Management, 171 , pp. 195 203 . doi: 10.1016/j.jenvman.2016.02.012

Brubaker D.R. and Claes Lykke Ragner, 'A review of the International Northern Sea Route Program (INSROP) – 10 years on', (2010) Polar Geography, Vol 33, Nos 1-2, pp. 15-38 http://dx.doi.org/10.1080/1088937X.2010.493308

Carmack, E., K. Aagaard, J. Swift, R. Perkin, F. McLaughlin, R. Macdonald,P. Jones, J. Smith, K.Ellis, and L.Kilius, Changes in temperature and tracer distributions within the Arctic Ocean: Results from the 1994 Arctic Ocean Section. Deep Sea Res., 44,1487-1502, 1997.

Dodd, P. A., B. Rabe, E. Hansen, E. Falck, A. Mackensen, E. Rohling, C. Stedmon, and S. Kristiansen (2012), The freshwater composition of the Fram Strait outflow derived from a decade of tracer measurements, J. Geophys. Res., 117, C11005, doi:10.1029/2012JC008011

Dodd, P.A., T. T. Blæsterdalen, M. Karcher and T. Hattermann, Pacific Water in the Arctic Ocean and East Greenland Current. In prep.

Ekwurzel B, Schlosser P, Mortlock RA, Fairbanks RG, Swift JH. River runoff, sea ice meltwater, and Pacific water distribution and mean residence times in the Arctic Ocean. J Geophys Res 2001;106:9075–92.

(Fimex 2020) Alexander Bürger, Heiko Klein; Fimex: File Interpolation, Manipulation and EXtraction library for gridded data; https://github.com/metno/fimex/releases/tag/v1.5.3

(Flaggbok 2014) Protective Measures in Early and Intermediate Phases of a Nuclear or Radiological Emergency; Nordic Guidelines and Recommendations DSA, STUK, SSM, SST, BRS, IRSA https://dsa.no/atomberedskap/hva-gjor-vi-pa-dsa/_/attachment/download/e951db09-7baf-43ca-baf1-eeade7bd7cce:83846c273090f076ee89e3e67f72c284e853a6d0/Nordisk%20flaggbok.pdf

Gerdes, R., Hurka, J., Karcher, M., Kauker, F., Koeberle, C. (2005). Simulated history of convection in the Greenland and Labrador seas 1948-2001, AGU monograph Climate Variability of the Nordic Seas, Bjerknes Centre for Climate Research, Bergen, Norway, 221-238.

Gerdes R., Karcher M., Kauker F. and Koeberle C. (2001): Prediction for the spreading of radioactive substances from the sunken submarine "Kursk" in the Barents Sea. EOS transactions, AGU, 82(23): 253-257.

Guemas, V., Blanchard-Wrigglesworth, E., Chevallier, M., Day, J. J., Déqué, M., Doblas-Reyes, F. J., Fučkar, N., Germe, A., Hawkins, E., Keeley, S., Koenigk, T., Salas y Mélia, D. and Tietsche, S. (2016) A review on Arctic sea ice predictability and prediction on seasonal-to-decadal timescales. Quarterly Journal of the Royal Meteorological Society, 142 (695). pp. 546-561. ISSN 1477-870X

Hersbach, H., Bell, B., Berrisford, P., Biavati, G., Horányi, A., Muñoz Sabater, J., Nicolas, J., Peubey, C., Radu, R., Rozum, I., Schepers, D., Simmons, A., Soci, C., Dee, D., Thépaut, J-N. (2018): ERA5 hourly data on pressure levels from 1979 to present. Copernicus Climate Change Service (C3S) Climate Data Store (CDS). (Accessed in 12-2020), 10.24381/cds.bd0915c6

Hibler W.D. III (1979): A dynamic thermodynamic sea ice model. Journal of Physical Oceanography, 1979, 9: 815-846.

Holloway, G., A. Nguyen, and Z. Wang (2007), Water properties and circulation in Arctic Ocean models, J. Geophys. Res., 112, C04S03, doi:10.1029/2006JC003642.

Jones, E. P., and L. G. Anderson (1986), On the origin of the chemical properties of the Arctic Ocean halocline, J. Geophys. Res., 91, 10,759–10,767

Kalnay, E., et al. (1996), The NCEP/NCAR 40-Year Reanalysis Project, Bull. Am. Meteorol. Soc., 77, 437 – 495.

Karcher, M. J., Gerdes, R., Kauker, F., Koeberle, C. (2003). Arctic warming - Evolution and Spreading of the 1990s warm event in the Nordic Seas and the Arctic Ocean, J. Geophys. Res., Vol. 108(C2), 3034.4

Karcher, M.J., S. Gerland, I. H. Harms, M. Iosjpe, H. E. Heldal, P. J. Kershaw and Sickel, M. (2004): The dispersion of 99Tc in the Nordic Seas and the Arctic Ocean: a comparison of model results and observations, J Environ Radioact, 74(1-3): 185-198.

Karcher, M., Gerdes, R., Kauker, F., K¨oberle, C., and Yashayaev, I.: Arctic Ocean change heralds North Atlantic freshening, Geophys. Res. Lett., 32, L21606, doi:10.1029/2005GL023861, 2005.

Karcher, M., Smith, J. N., Kauker, F., Gerdes, R., & Smethie, W. M. (2012). Recent changes in Arctic Ocean circulation revealed by iodine-129 observations and modeling. J. Geophys. Res. Oceans, (1978–2012), 117(C8).

Karcher, M., Gerdes, R., Kauker, F. (2008). Long-term variability of Atlantic water inflow to the Northern Seas: insights from model experiments, Arctic-Subarctic Ocean Fluxes: Defining the role of the Northern Seas in Climate, Editors: B. Dickson, J. Meincke and P. Rhines, Springer.

Karcher, M., T. Hattermann, P. A. Dodd and T. T. Blæsterdalen, Comparison of Modeled Transports of Freshwater Fractions and Tracer-Derived Observations of Freshwater Fractions under various atmospheric conditions.. In prep.

Karcher, M. , Hosseini, A. , Schnur, R. , Kauker, F. , Brown, J. , Dowdall, M. and Strand, P. (2017): Modelling dispersal of radioactive contaminants in Arctic waters as a result of potential recovery operations on the dumped submarine K 27 , Marine Pollution Bulletin, 116 (1 2), pp. 385 394 . doi: 10.1016/j.marpolbul.2017.01.034

Kauker, Frank, et al., 2003. Variability of Arctic and North Atlantic sea ice: a combined analysis of model results and observations from 1978 to 2001. J. Geophys. Res. Oceans (1978e2012) 108 (C6).

Kauker, F. , Kaminski, T. , Karcher, M. , Dowdall, M. , Brown, J. , Hosseini, A. and Strand, P. (2016): Model analysis of worst place scenarios for nuclear accidents in the Northern marine environment , Environmental Modelling & Software, 77 , pp. 13 18 . doi: 10.1016/j.envsoft.2015.11.021

Köberle, C., and R. Gerdes (2003), Mechanisms determining the variability of Arctic sea ice conditions and export, J. Clim., 16: 2843–2858, doi:10.1175/1520-0442.

McLaughlin, F. A., E. C. Carmack, R. W. Macdonald, and J. K. B. Bishop (1996), Physical and geochemical properties across the Atlantic/Pacific water mass in the Southern Canadian Basin, J. Geophys. Res., 101, 1183–1197.

Pacanowski, R. C. (1995), MOM 2 Documentation, user's guide and reference manual, GFDL Ocean Group Tech. Rep. 3, Geophys. Fluid Dyn. Lab., Princeton Univ., Princeton, N. J..

Proshutinsky, A., R. Krishfield, M.-L. Timmermans, J. Toole, E. Carmack, F. McLaughlin, W. J. Williams, S. Zimmermann, M. Itoh, and K. Shimada (2009), Beaufort Gyre freshwater reservoir: State and variability from observation, J. Geophys. Res., 114, C00A10, doi:10.1029/2008JC005104. (Printed 115(C1), 2010.)

Serreze, M.C. and Julienne Stroeve (2015) Arctic sea ice trends, variability and implications for seasonal ice forecasting373Philosophical Transactions of the Royal Society A: Mathematical, Physical and Engineering Scienceshttp://doi.org/10.1098/rsta.2014.0159

(SNAP 2011) Bartnicki, J, Haakenstad, H., Hov, Ø,;Operational SNAP Model for Remote Applications From NRPA; met.no Report no. 12/2011Air Pollution ISSN: 332-9879 https://drive.google.com/file/d/0B8SjSRklVkHkQXoxY1VQdE0wdnM/

(SNAP 2021) Klein, Heiko & Ulimoen, Magnus. (2021). metno/snap: (Version v2.0.3-pevek). https://github.com/metno/snap/releases/tag/v2.0.3-pevek

Smith, J. N., K. M. Ellis, and L. R. Kilius (1998), 129I and 137Cs tracer measurements in the Arctic Ocean, Deep Sea Res., 45, 959–984, doi:10.1016/S0967-0637(97)00107-6.

Smith, J. N., K. M. Ellis, and T. M. Boyd (1999), Circulation features in the central Arctic Ocean revealed by nuclear fuel reprocessing tracers from SCICEX 95 and 96, J. Geophys. Res., 104, 29,663–29,677, doi:10.1029/1999JC900244.

Smith, J. N., F. A. McLaughlin, W. M. Smethie Jr., S. B. Moran, and K. Lepore (2011), Iodine-129, 137Cs, and CFC-11 tracer transit time distributions in the Arctic Ocean, J. Geophys. Res., 116, C04024, doi:10.1029/2010JC006471.

Steele, M., R. Morley, and W. Ermold (2001), PHC: A global ocean hydrography with a high quality Arctic Ocean, J. Clim., 14: 2079 – 2087.

Steele, M., J. Morison, W. Ermold, I. Rigor, M. Ortmeyer, and K. Shimada (2004), Circulation of summer Pacific halocline water in the Arctic Ocean, J. Geophys. Res., 109, C02027, doi:10.1029/2003JC002009.

Stewart, K.D., Haine, T.W.N., 2013. Wind-driven Arctic freshwater anomalies. Geophys.Res. Lett. 40. http://dx.doi.org/10.1002/2013GL058247.

Stevens, D.P. (1991) The Open Boundary Condition in the United Kingdom Fine-Resolution Antarctic Model. Journal of Physical Oceanography, 21 (9): 1494-1499.

⫙ DSA